INVESTIGATION OF SUPERSONIC PROJECTILE DRAG REDUCTION USING BASE INJECTION AND FREE STREAM COMBUSTION

Noel Paul Horn

NAVAL POSTGRADUATE SCHOOL
Monterey, California

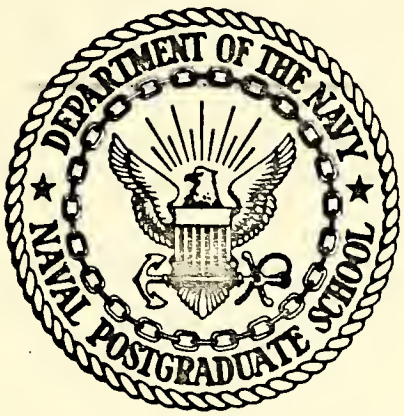

THESIS

INVESTIGATION OF SUPERSONIC PROJECTILE DRAG REDUCTION USING BASE INJECTION AND FREE STREAM COMBUSTION

by

Noel Paul Horn

Thesis Advisor: Allen E. Fuhs

March 1974

Investigation of Supersonic Projectile Drag Reduction Using Base Injection and Free Stream Combustion

by

Noel Paul Horn
Lieutenant, United States Navy
B.S., United States Naval Academy, 1967

Submitted in partial fulfillment of the
requirements for the degree of

MASTER OF SCIENCE IN AERONAUTICAL ENGINEERING

from the

NAVAL POSTGRADUATE SCHOOL
March 1974

ABSTRACT

Base drag accounts for nearly half the total drag of a supersonic projectile. A review is presented of early base flow studies. By relating rate of entropy generation to projectile drag, it is demonstrated that the trailing shock dominates base drag. Base injection was selected as the means of weakening this shock. Base pressure, as a function of injectant flow rate, was obtained by means of a free jet wind tunnel with a coaxial, Mach 2.0 nozzle. Base pressure ratio (P_B/P_∞) increases of 13 percent at an effective I_{SP} of 465 seconds were achieved with cold nitrogen. Free stream combustion was simulated by nozzle contour. Base pressure increases due to free stream combustion and base injection were shown not to be additive effects.

TABLE OF CONTENTS

LIST OF TABLES

LIST OF FIGURES

NOTATIONS

English

A	area
C	chord of body
D	drag
h	half width of body
I_{sp}	specific impulse
l_{ab}	length along oblique shock from axis of symmetry to last expansion wave
M	Mach number
$\dot{m}$	mass flux
P	pressure
Re_{∞}	free stream Reynolds number based on body thickness
Re_{inj}	injectant Reynolds number based on injection port diameter
Region 1	region between expansion fan and trailing shock
Region 2	region downstream of trailing shock
$\dot{S}$	entropy generation rate
S*	nondimensional entropy generation rate
T	temperature
U	velocity
u(y)	velocity profile

Greek

α	expansion angle of free shear layer and wake
β	angle between oblique shock and upstream flow
γ	specific heats ratio
$\delta(x)$	boundary layer thickness distribution

δ_B	boundary layer thickness approaching base
θ	turning angle of flow through expansion fan
μ	fluid viscosity
ρ	fluid density

Subscripts

0	conditions when Re = 10^6
1	within region 1
2	within region 2
∞	free stream conditions
B	base conditions
INJ	injectant conditions
T	total or stagnation

ACKNOWLEDGEMENT

The author wishes to express his gratitude to Professor A. E. Fuhs for his unending patience and guidance as thesis advisor. The author would also like to express his thanks to CDR W. J. H. Smithey for his assistance and, finally, to Messers. J. Moulton and N. Leckenby for their technical help.

I. INTRODUCTION

The typical projectile traveling at supersonic speeds is subjected to three major components of drag: wave drag, skin friction, and base pressure drag. Wave drag, comprising about half the total drag, may be reduced by design of low-drag shapes. This has been a topic of study for many years. Skin friction drag, which is only on the order of 1 percent of the total drag, [Ref. 1] is not a serious area of concern. Base drag, on the other hand, comprises about one-half the total drag and is our topic of study.

Historically, the reduction of base drag has been attempted by the use of streamlined or boat tailed projectiles. These approaches, although partially alleviating the problem, have resulted in poor longitudinal stability characteristics. This leaves a great deal of room for improvement [Ref. 2].

Recent studies have shown the effectiveness of external burning in alleviation of the base drag problem. This is accomplished by the generation of compression waves which impinge on the base flow area and increase base pressure. Mass injection into the base flow area distorts the shape of this region and results in a flow pattern more conducive to increased base pressure.

A combination of burning in both the base flow region and the free stream affords a promising possibility for improvement of gun system potential.

II. EARLY BASE FLOW STUDIES

One of the earliest concise statements of the nature of supersonic base flow was made by Chapman [Ref. 3] in 1950.

A. TWO-DIMENSIONAL INVISCID

The simplest problem of this nature is two-dimensional inviscid flow over a semi-infinite rearward-facing step as shown in Fig. 1.

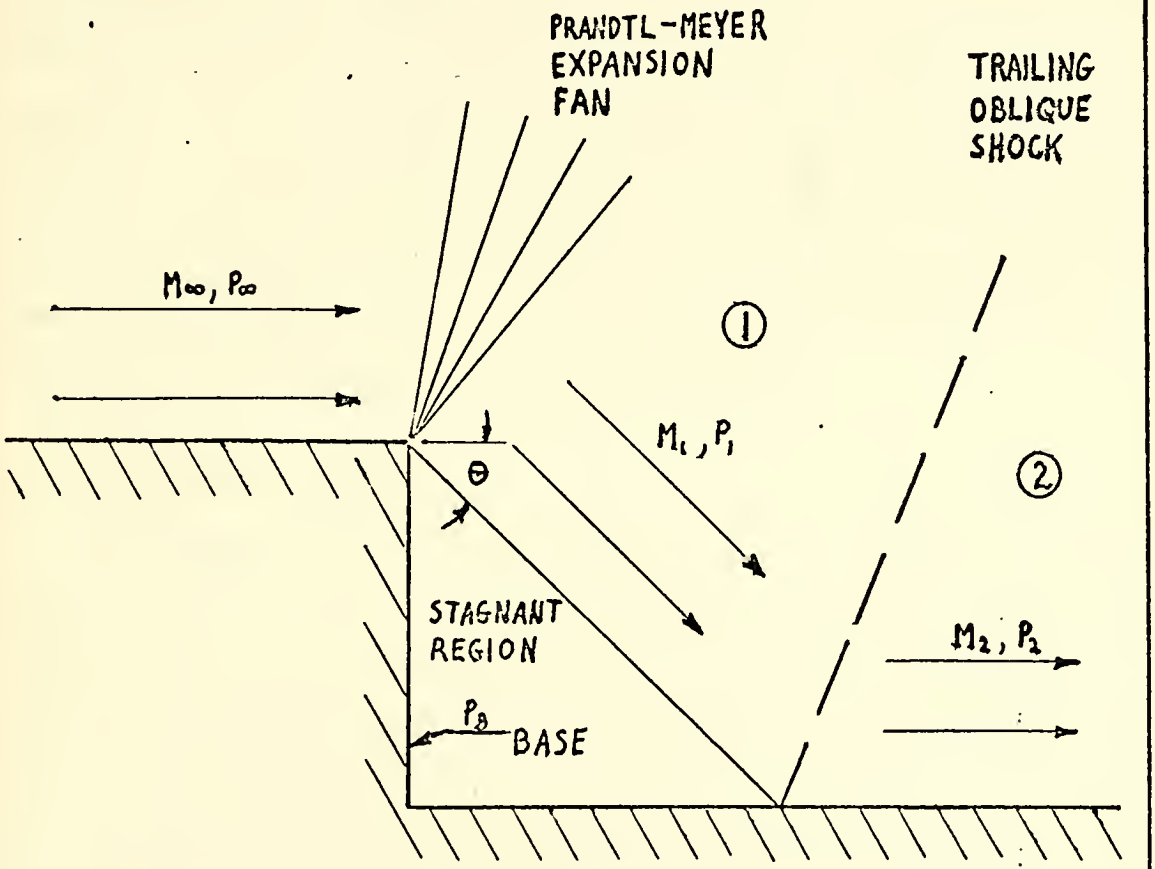

Fig 1

INVISCID SUPERSONIC FLOW OVER A STEP

As the supersonic free stream, M_∞, approaches the base area of the step, a deflection of the flow is required to fill the downstream region. This is accomplished by the Prandtl-Meyer expansion fan. The flow in region 1 has been turned through an angle θ. The Mach number of region 1, M_1, is greater than that of the free stream, M_∞, while the pressure, P_1, is less than that of free stream, P_∞. A final deflection of the flow to parallel free stream is performed by the trailing oblique shock. Downstream Mach number, M_2, and pressure, P_2, approach free stream conditions. The base pressure, P_B, or pressure in the stagnant region is equal to P_1.

For given free stream conditions, P_∞ and M_∞, together with a value of P_B, we may compute a unique expansion angle, θ. This same angle will determine properties of the trailing shock. If we are given only free stream conditions, we are allowed an infinite number of solutions combining turning angles and base pressures. The only limitation appears to be the ability of a single oblique shock to redirect the expanded flow parallel to the free stream. It is apparent that the inviscid model is an inadequate simulation for problem under study.

B. AXISYMMETRIC INVISCID

Axisymmetric inviscid flow is shown in Fig. 2. Such flow is more complex since the expansion fan and the streamlines of region 1 are curved. Flow properties may be computed using the method of characteristics. The curved streamlines of region 1, if continued to the body axis of symmetry, would require a turning angle too large for one oblique shock to accomplish. For this reason the shock moves upstream to an equilibrium position. A wake area is then assumed where the shock cannot exist. As in the two-dimensional case, the flow in region 2 parallels free stream and approaches the same pressure and Mach number. As in the two-dimensional

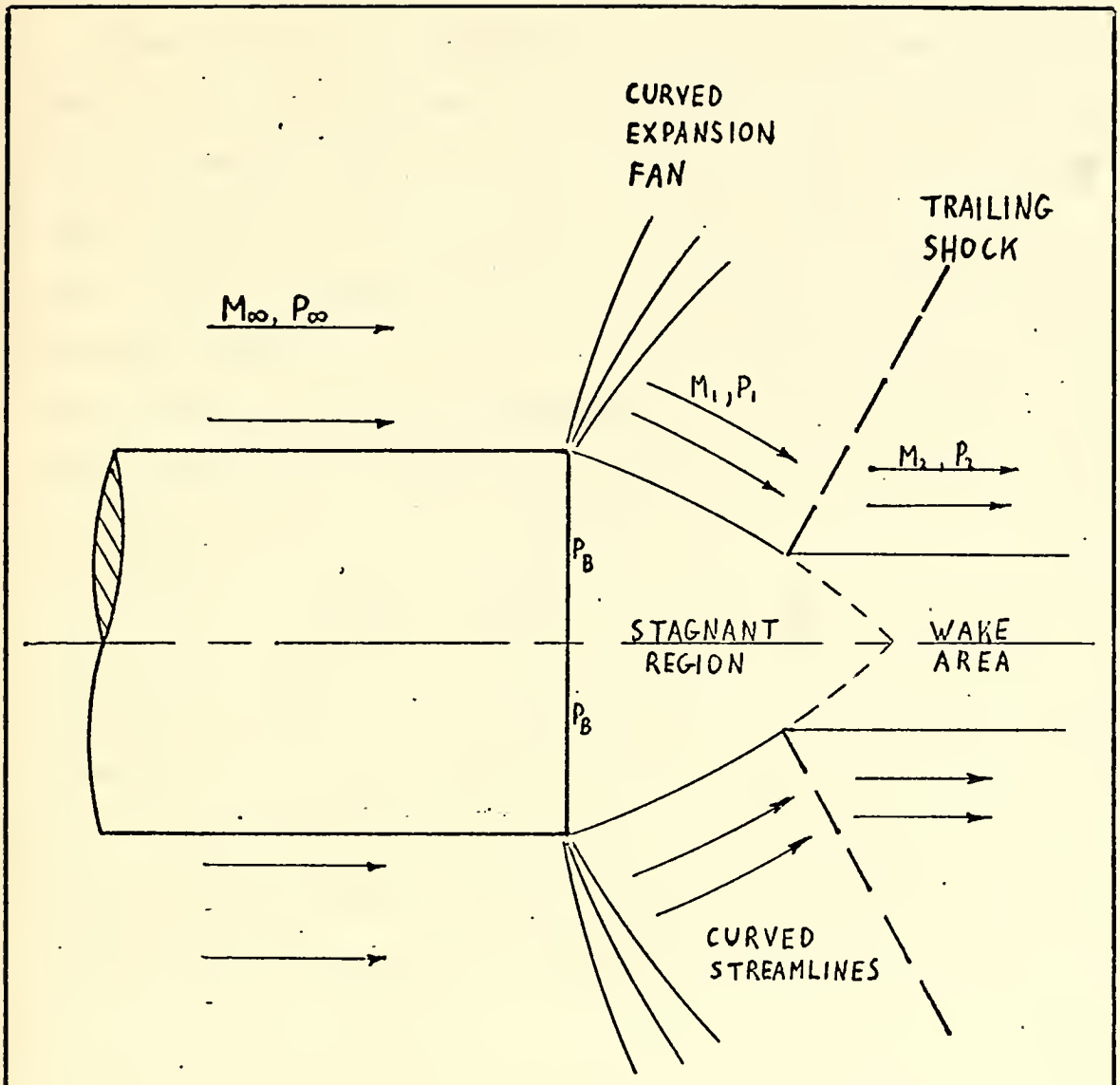

Fig 2

AXISYMMETRIC INVISCID SUPERSONIC FLOW

case, an infinite number of flow solutions exist given a set of free stream conditions, each corresponding to a selected base pressure.

C. VISCOUS EFFECTS

Figure 3 illustrates the features of axisymmetric base flow with viscous effects. In this case, a finite boundary layer of thickness δ_B approaches the base region. After the expansion there is found a free shear layer expanding in size. A wake area is located after the trailing shock. Due to the viscous effects of the free shear layer, the fluid immediately behind the body is no longer stagnant, becoming instead a zone of slow recirculating flow. Air is scavenged from this recirculation zone by the free shear effects. Stagnation points are located at A and B within the recirculation zone.

As air is scavenged from the recirculation zone, the expansion angles of the flow increase. A shock of increased strength and pressure rise limits the amount of low energy air removed. This provides an equilibrium condition and a unique solution to the base flow problem. Unfortunately such viscous theory is far too complex to be of practical value in predicting base pressures. Chapman's attempts to correlate base pressure with Reynolds number met with but limited analytical success [Ref. 3].

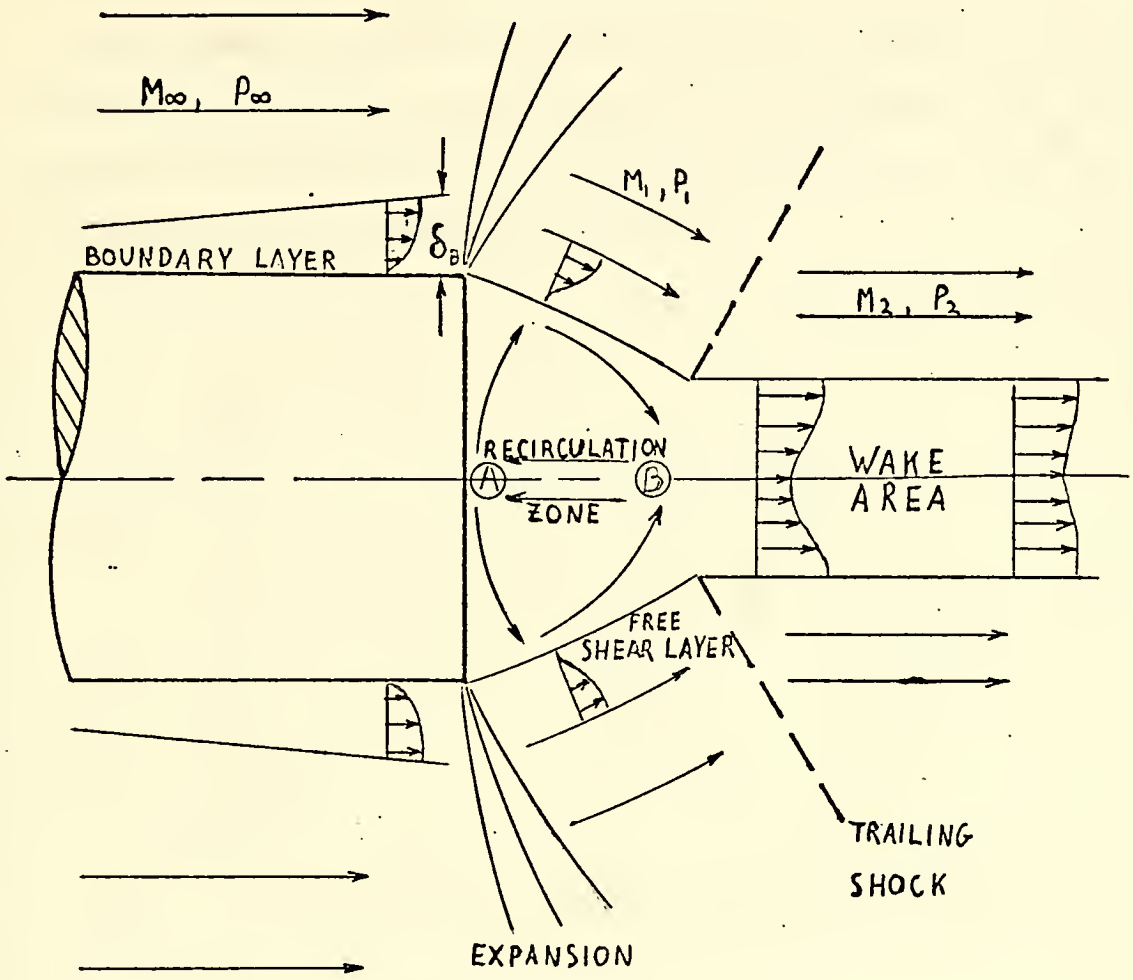

Fig 3

VISCOUS EFFECTS

III. ENTROPY PRODUCTION IN BASE FLOW

A. FLAT PLATE ANALOGY

In most physical processes, associated losses or inefficiencies may be related to the rate of entropy generation. An example follows using the laminar boundary layer on a flat plate as shown by Schlicting [Ref. 4]. The Blasius profile is assumed in Fig. 4.

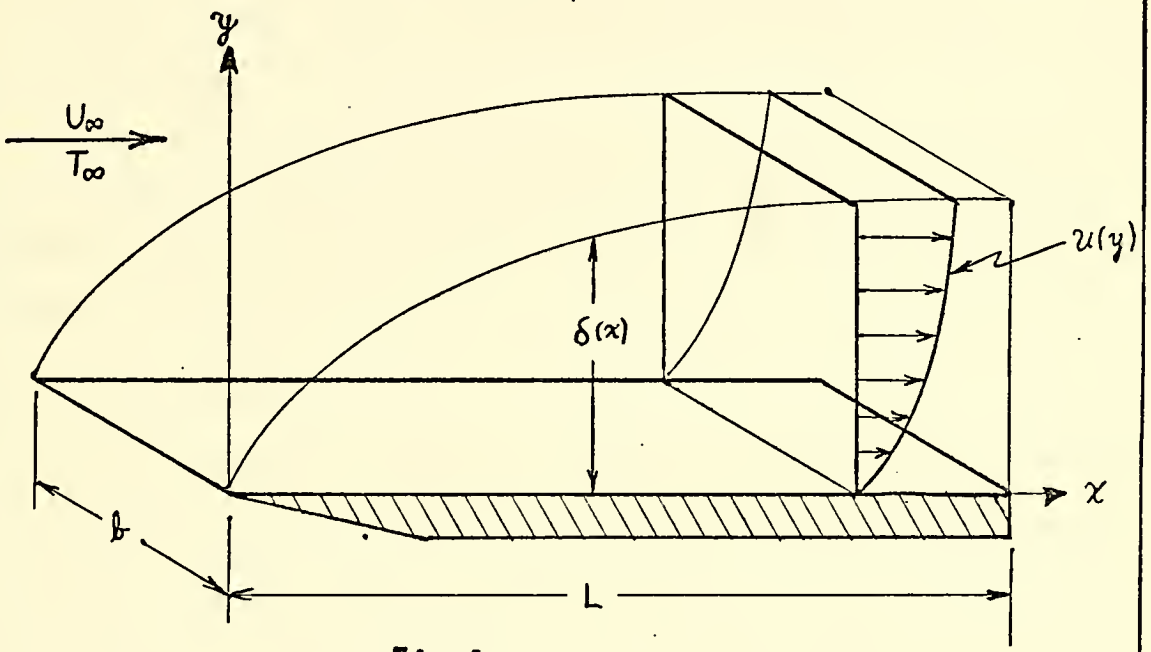

Fig 4

LAMINAR PROFILE ON A FLAT PLATE

Entropy generation, $\dot{S}$, may be nondimensionalized with respect to kinetic energy flux giving:

$$S^* = \frac{\dot{S}\, T_\infty}{\rho_\infty U_\infty^3\, bL} = \frac{\mu}{\rho U^3\, bL} \int_0^L \int_0^\delta \frac{1}{\delta(x)} \left(\frac{\partial(\frac{u}{U_\infty})}{\partial(y/\delta)}\right)^2 d(y/\delta)\, dx \qquad (1)$$

Defining $u' = u/U_\infty$, $y' = y/\delta$ and unit width of the flat plate:

$$S^* = \frac{\mu}{\rho UL} \int_0^L \int_0^1 \left(\frac{\partial u'}{\partial y'}\right)^2 dy'dx \qquad (2)$$

Using Reynolds number based on plate length, $Re_L = \rho_\infty U_\infty L/\mu_\infty$ and Schlicting's relationship, $\delta(x) = 5x/\sqrt{Re_x}$

$$S^* = \frac{1}{Re_L} \int_0^L \frac{\sqrt{Re_x}}{5x}\, dx \int_0^1 \left(\frac{\partial u'}{\partial y'}\right)^2 dy' \qquad (3)$$

When properly integrated it may be shown that $S^* = .664/\sqrt{Re_L}$. Entropy generated by total drag, D, may be similarly related by $\dot{S} = DU_\infty/T_\infty$ where $DU_\infty/T_\infty = .664\, \rho\, U_\infty^2\, bL/Re_L$ giving again $S^* = .664/\sqrt{Re_L}$.

These discussions show the general relationship between entropy generation and drag due to shear. There is no value to which S* converges as drag increases.

B. ANALYTIC MODEL

A two-dimensional model will be derived to show qualitative effects of viscous base flow. The three major contributions to entropy generation in the base flow are from the free shear layer, the wake, and the trailing shock shown in Fig. 5. This model corresponds to data gleaned from Ref. 3, where a wedge is immersed in a supersonic flow of air. Properties of the experiments shown include wedge half height to chord ratio, h/c, of .0375, Reynolds number based on chord, $Re_c = 10^6$, $M_\infty = 2.0$, and ratio of specific heats for air = 1.4. Attention will be given to each of the above drag components.

1. Free Shear Layer

The proposed model of the free shear layer is shown in Fig. 6. The assumptions applicable to this model follow:

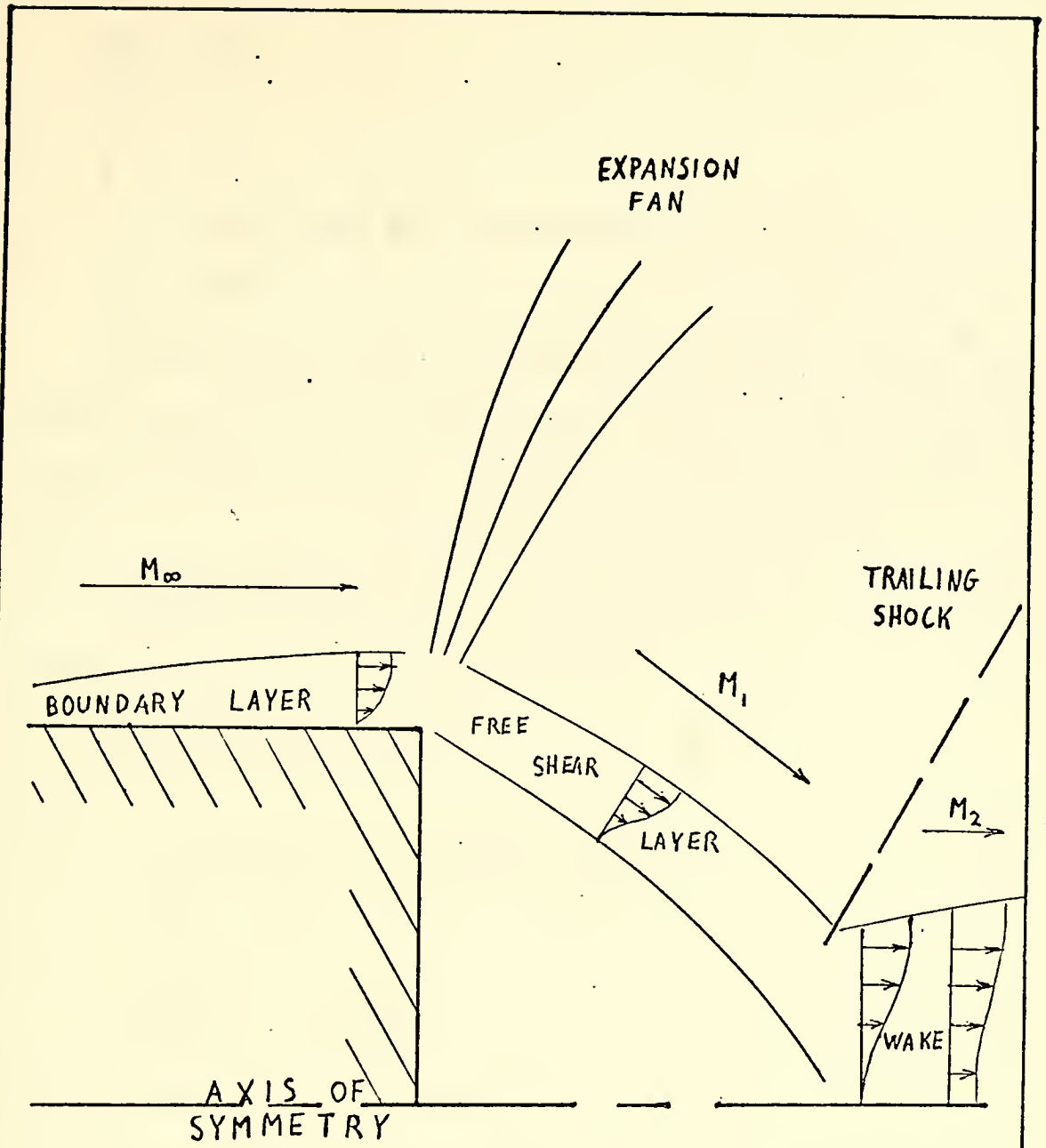

Fig 5

ENTROPY FROM VISCOUS FLOW

$Re = 10^6$

$h/c = .0375$

$M = 2.0$

$\gamma = 1.4$.

$L = h \csc\theta$ where θ = deflection angle

$X_0 = \delta_B/2\alpha$

Free shear layer width is αX, where $\alpha = \alpha_0 \sqrt{Re_c}/10^6$, and $\alpha_0 = 3^\circ$.

The free shear velocity profile, $U(X,Y)$, is $(U_1/2)(1-\cos(\pi Y/\alpha X))$, where U_1 is the region 1 velocity. Returning to the flat plate analogy:

$$\dot{S} = \int_X \int_Y \frac{\mu}{T_1} \left(\frac{\partial u}{\partial Y}\right)^2 dY\, dX \tag{4}$$

where:

$$\frac{\partial u}{\partial Y} = (U_1 \pi/2\alpha X)\sin(\pi Y/\alpha X)$$

So:

$$\dot{S} = \int_{X_0}^{h \csc\theta} \frac{\mu}{T_1} \frac{U_1^2}{4} \left(\frac{\pi}{\alpha X}\right)^2 \int_0^{\alpha X} \sin^2\left(\frac{\pi Y}{\alpha X}\right) dY\, dX \tag{5}$$

or:

$$\dot{S} = \frac{\mu U_1^2 \pi^2}{T_1 8\alpha} \ln\left(\frac{2\alpha \csc\theta}{\delta/h}\right) \tag{6}$$

By nondimensionalizing one achieves:

$$S^* = \frac{T_\infty}{T_1} \left(\frac{U_1}{U_\infty}\right)^2 \frac{\mu}{\rho_\infty U_\infty h} \frac{\pi^2}{8\alpha} \ln\left(\frac{2\alpha \csc\theta}{\delta/h}\right) \tag{7}$$

Upon substitution of initial values and assumptions the nondimensionalized entropy generation takes its final form:

$$S^* = \frac{\pi^2}{8000} \frac{1}{\alpha_0} \left(\frac{M_1}{M_\infty}\right)^2 \frac{c}{h} \frac{1}{\sqrt{Re_\infty}} \ln(15\alpha_0 \csc\theta) \tag{8}$$

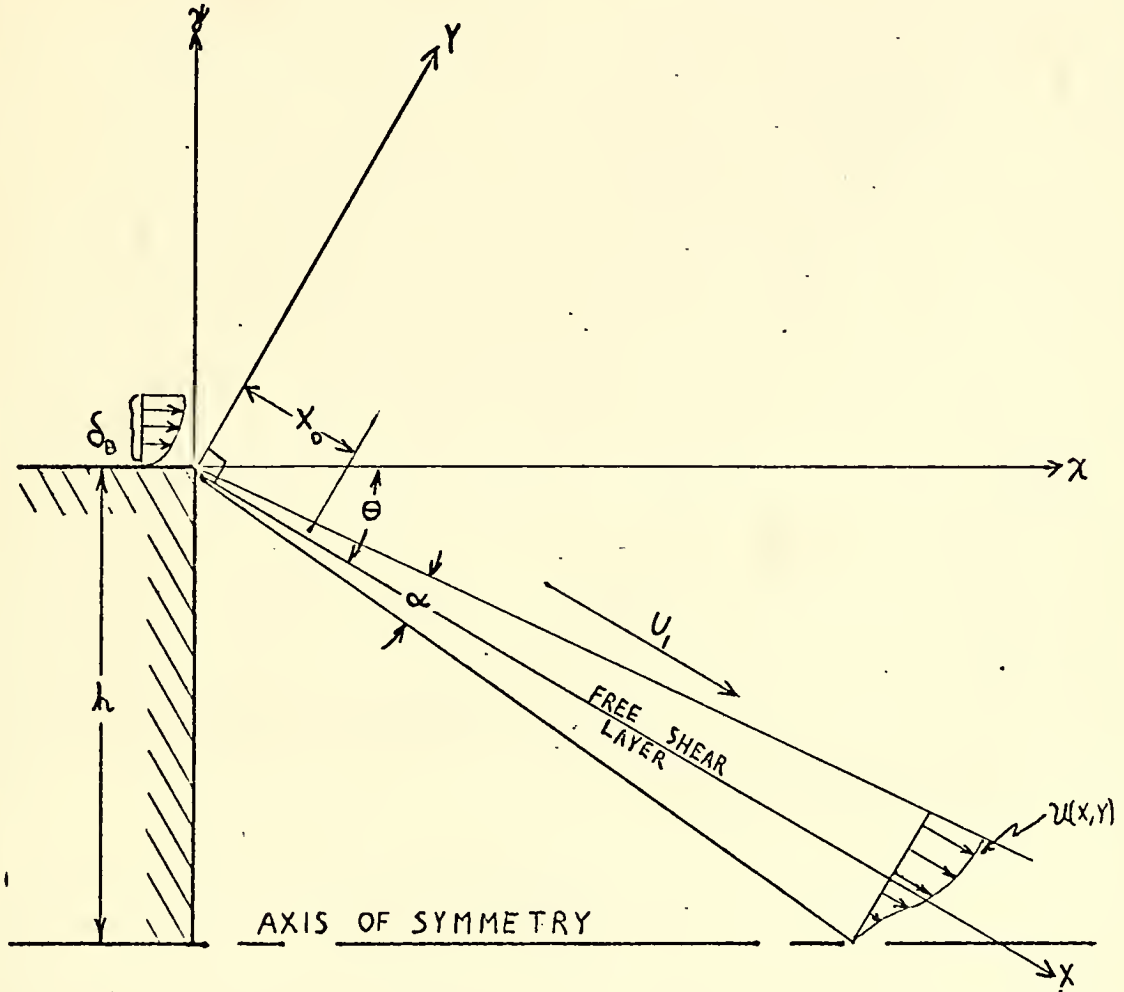

Fig 6

FREE SHEAR MODEL

2. Wake Area

The proposed model of the wake area is shown in Fig. 7.

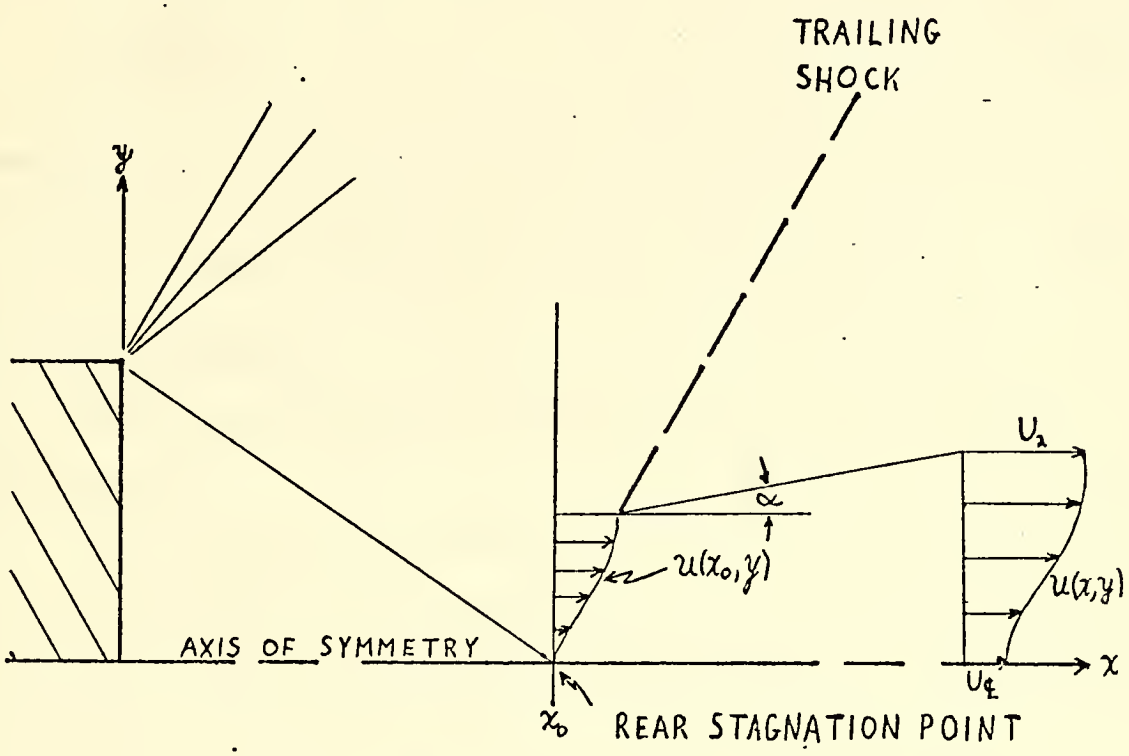

Fig 7

WAKE MODEL

Definitions and assumptions include:

x_0 = stagnation point

U_ℓ = centerline velocity (along axis of symmetry)

α = expansion angle of shear layer as determined previously

u = velocity in shear layer = $U_\ell(x)+\frac{1}{2}(U_2-U_\ell)(1-\cos(\pi y/\alpha x))$ where

$U_\ell = U_2(1-x_0/x)$

So:

$$u(x,y) = U_2 - (U_2 x_0/2x)(1+\cos \frac{\pi y}{\alpha x}) \tag{9}$$

and

$$\partial u/\partial y = (U_2 x_0 \pi/2\alpha x^2) \sin (\pi y/\alpha x)$$

$$\dot{S} = \int_x \int_y (\frac{\partial u}{\partial y})^2 \frac{\mu}{T_2} \, dx \, dy \tag{10}$$

$$\dot{S} = \frac{\pi^2 U_2^2 \mu}{8\alpha T_2} \tag{11}$$

Finally, nondimensionalization gives:

$$S^* = \frac{c}{h} \frac{1}{\sqrt{Re_\infty}} (\frac{M_2}{M_\infty})^2 \frac{\pi^2}{8000\alpha_0} \tag{12}$$

3. Shock Entropy

The proposed model for the trailing shock is shown in Fig. 8. In this figure:

μ_1 = Mach angle for region 1

θ = flow deflection angle

β = shock angle relative to region 1 flow

h = half width of body

a,b = end points for full strength area of trailing shock

The length of this full strength zone for the trailing shock, l_{ab}, is denoted by:

$$l_{ab} = h \frac{\cot(\mu-\theta) + \cot\theta}{\sin(\beta-\theta)\cot(\mu-\theta) - \cos(\beta-\theta)} \tag{13}$$

Entropy generation is obtained from normal shock relations and is found to be:

$$\dot{S} = \rho_1 U_1 \sin\beta \, l_{ab} \, R \ln (\frac{P_{01}}{P_{02}}) \tag{14}$$

Finally:

$$S^* = \frac{\rho_1}{\rho_\infty} \frac{U_1}{U_\infty} \frac{1}{\gamma M_\infty^2} \frac{l_{ab}}{h} \sin\beta \ln (\frac{P_{01}}{P_{02}}) \tag{15}$$

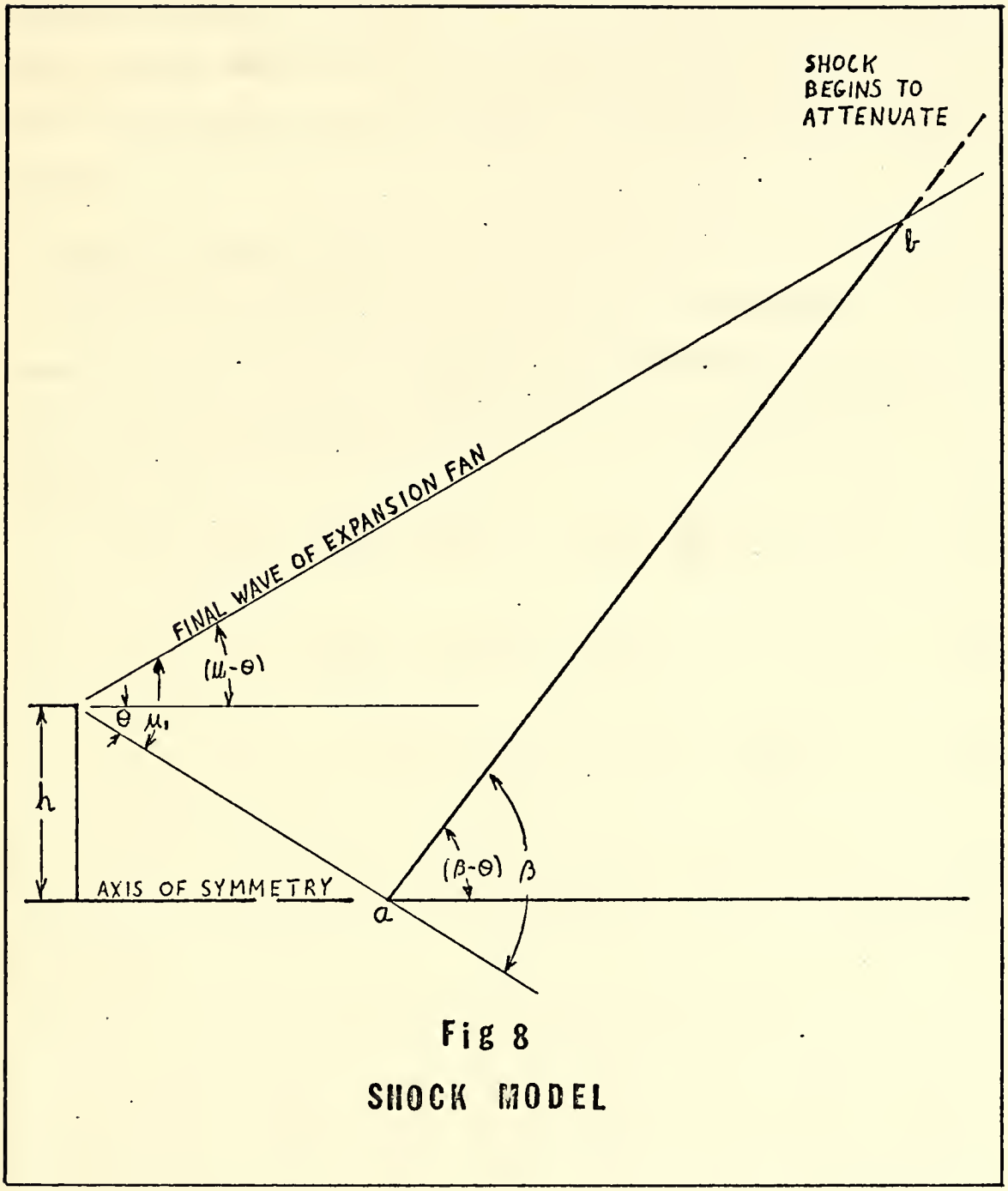

Fig 8

SHOCK MODEL

It should be noted that this value of entropy generation does not take into account the regions where the strength of the trailing shock begins to attenuate. Also the shock is assumed to occur at full strength to the plane of symmetry. Since the shock wave beyond the first characteristic of the fan is neglected, exact comparison between base drag and the model is not possible. However, trends due to influence of Re and M are correct.

C. RESULTS OF ENTROPY STUDY

As has been shown earlier, the total rate of nondimensional entropy generation due to base drag, $S^*_{\text{base drag}}$, is comprised of $S^*_{\text{free shear}}$, S^*_{wake}, and $S^*_{\text{trailing shock}}$. These previously derived quantities are evaluated below:

$$S^*_{\text{free shear}} = \frac{\pi^2}{8000} \frac{1}{\alpha_0} \left(\frac{M_1}{M_\infty}\right)^2 \frac{c}{h} \frac{1}{\sqrt{Re_\infty}} \ln(15\alpha_0 \csc\theta) \qquad (8)$$

$$S^*_{\text{wake}} = \frac{\pi^2}{8000} \frac{1}{\alpha_0} \left(\frac{M_2}{M_\infty}\right)^2 \frac{c}{h} \frac{1}{\sqrt{Re_\infty}} \qquad (12)$$

$$S^*_{\text{trailing shock}} = \frac{\rho_1}{\rho_\infty} \frac{U_1}{U_\infty} \frac{1}{\gamma M_\infty^2} \frac{l_{ab}}{h} \sin\beta \ln \frac{P_{01}}{P_{02}} \qquad (15)$$

Table I below illustrates the effects of each entropy source and its contribution to total drag as the flow deflection angle, θ, is varied with $Re_\infty = 10^6$.

TABLE I. ENTROPY CONTRIBUTIONS, $Re = 10^6$

θ°	5	10	12	15	17	20	25
$S^*_{\text{free shear}}$	.00166	.00135	.00127	.00118	.00112	.00105	.00093
S^*_{wake}	.00061	.00060	.00060	.00059	.00058	.00056	.00051
S^*_{shock}	.01648	.02692	.02963	.03190	.03328	.03382	.03341
S^*_{total}	.01875	.02887	.03150	.03367	.03498	.03543	.03485

To demonstrate the effect of free stream Reynolds number, the following table illustrates entropy generation rates for $Re_\infty = 10^5$.

TABLE II. ENTROPY CONTRIBUTIONS, Re = 10^5

θ^o	5	10	12	15	17	20	25
$S^*_{\text{free shear}}$	.00524	.00423	.00401	.00373	.00354	.00332	.00294
S^*_{wake}	.00193	.00190	.00190	.00186	.00183	.00177	.00161
S^*_{shock}	.01648	.02692	.02693	.03190	.03328	.03382	.03341
S^*_{total}	.02365	.03305	.03284	.03749	.03865	.03891	.03796

These tables with the aid of Fig. 9 demonstrate readily the small effects of Reynolds number and the complete domination of the base drag problem by the trailing shock effects.

From the above figure, it may be seen that decreasing the free stream Reynolds number by a factor of 10 affects only the free shear and wake effects. Such entropy increases amount to 10 percent to 25 percent of the total. By altering θ, on the other hand, entropy increases of nearly 200 percent are observed due to the changes in trailing shock strength.

It would appear reasonable to assume that steps to decrease the strength of the trailing shock would result in decreases in the base drag. The method proposed is to decrease the turning angles of the flow by altering the properties of the recirculating flow area. This promises to provide the desired weakening of the trailing shock and significant base drag reduction.

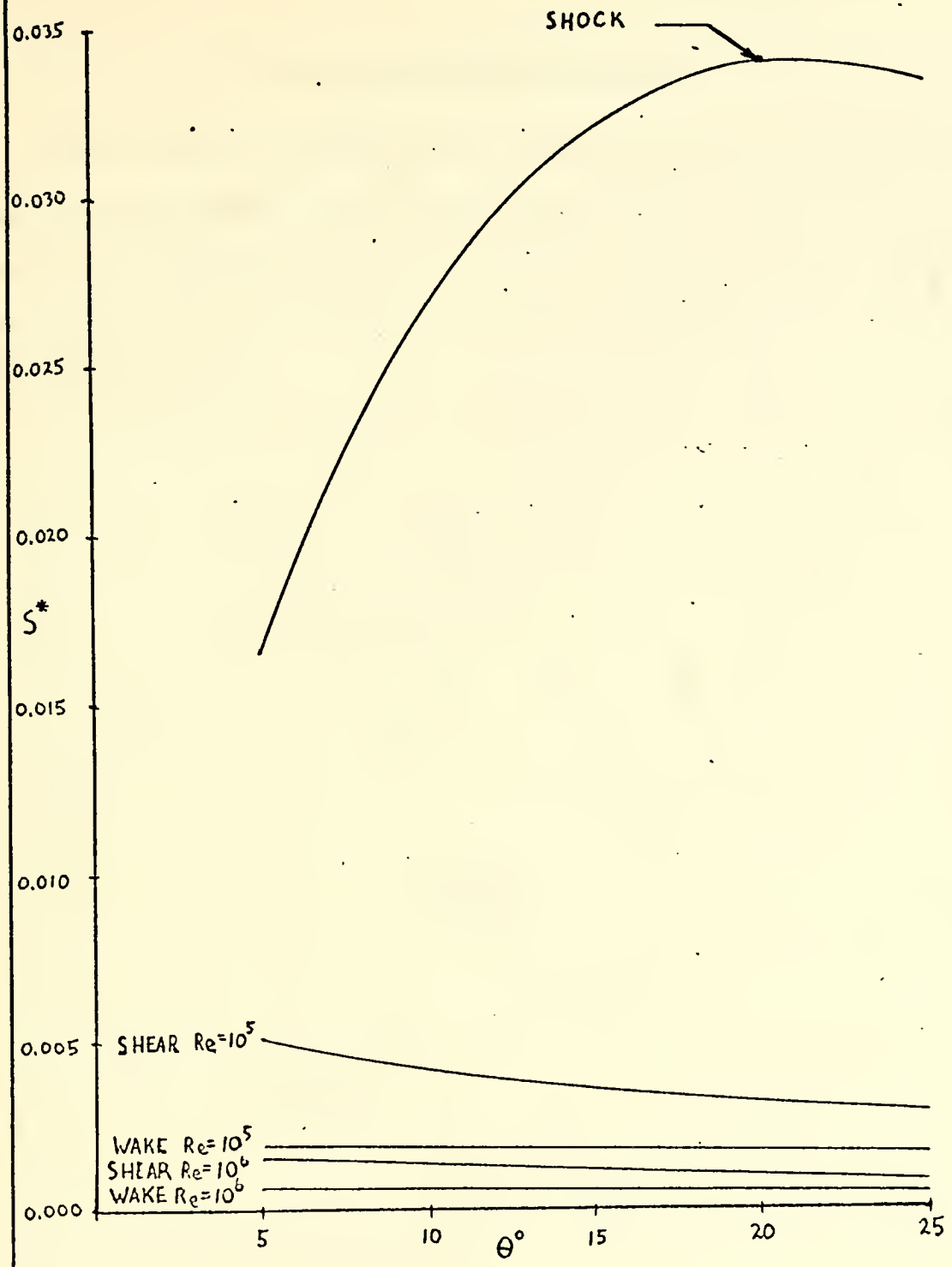

Fig 9

PLOT OF ENTROPY STUDY

IV. FREE STREAM COMBUSTION EFFECTS

Strahle [Ref. 5] and Fuhs [Ref. 6] demonstrated how compression waves may be generated from a supersonic combustion zone. This principle was applied by Caswell [Ref. 7] and Naber [Ref. 8] to increase the base pressure of a projectile in supersonic flight. A schematic of their method is shown in Fig. 10.

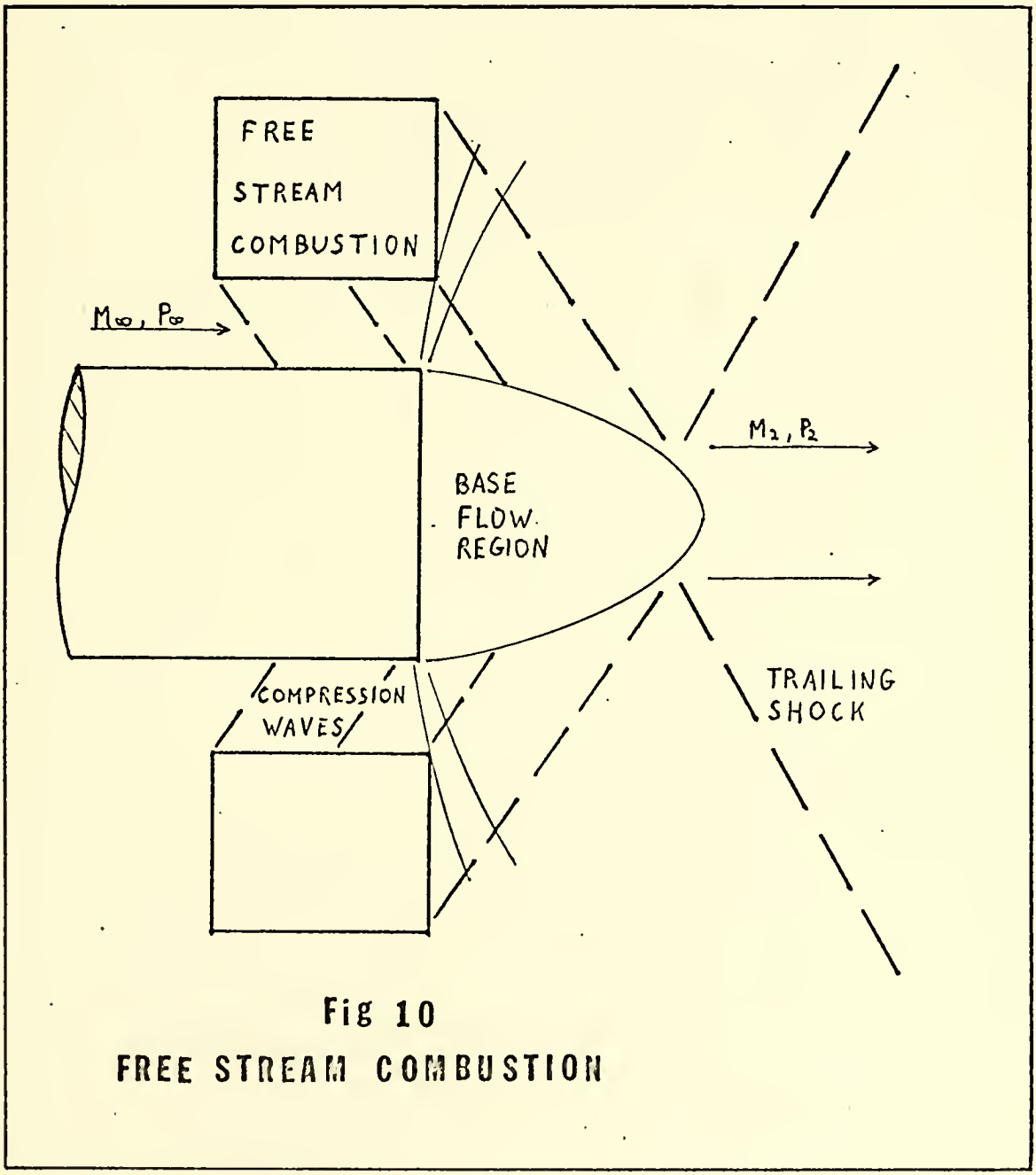

Fig 10
FREE STREAM COMBUSTION

Compression waves generated by the free stream combustion zones impinge upon the base flow region, providing a significant increase in base pressure. Experiments have shown that such compression waves may completely eliminate base drag or even provide a net thrust to this region.

V. BASE INJECTION AND COMBUSTION

As has been mentioned earlier, one promising area for study in reducing base drag is alteration of the base flow region in such a manner as to weaken the strength of the trailing shock. Sedney [Ref. 2] noted that base drag comprises nearly 50 percent of the total drag for typical low drag shapes and in some practical cases increases to 70 percent of the total. After noting that suitable analytical methods did not exist for handling base flows, he observed that total drag reductions of 14 percent were attained by artillery rounds with tracers in the base. Since momentum flux from a tracer is negligible, the gas generated by combustion must have performed the desired disruption of the base flow and led to the observed reduction in drag.

Collins, et al. [Ref. 9] studied effects of mass injection in the two-dimensional case and concluded that in this case the ratio of momentum flux of injectant to that of the boundary layers of the body was a dominating influence. This would seem to conflict with Sedney's observations. It should be noted, however, that comparisons between two-dimensional and axisymmetric flow may not be valid.

Detailed experimental studies of supersonic wedge flows with varying injection parameters were performed by Lewis and Chapkis [Ref. 10]. Figure 11 illustrates their findings in a qualitative manner.

The base flow region with no mass injection had two stagnation points, one at the rear of the recirculation region and one at the rear of the body itself. As injectant is added to the base region, the forward stagnation point is driven aft from the body. Increasing injection rates continue to move the forward stagnation point toward the rear point.

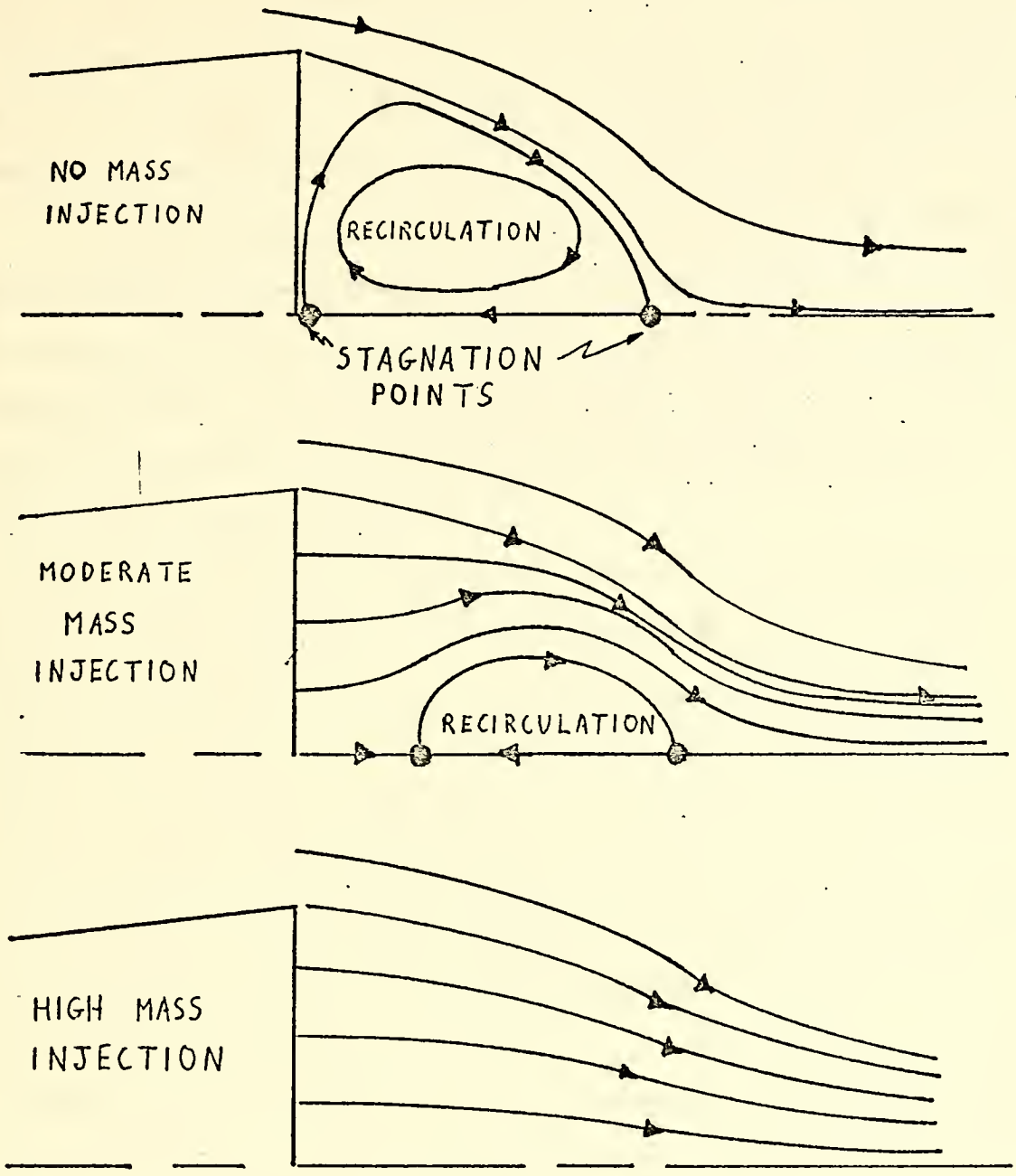

FIG 11
BASE INJECTION

Eventually these two points coincide. A further increase of injectant will result in complete loss of the recirculation region. This is, in effect, a rocket-type base flow. These studies also showed that addition of injectant resulted in base drag reductions far in excess of the momentum flux of the injectant. This again would seem to indicate that drag reductions were accomplished by disruptions of the base flow field.

As determined earlier, it appears that fluid is removed from the recirculating region by scavenging action of the free shear layer. Addition of injectant should result in the removal of more fluid by these finite shearing actions. It is proposed that increased injection will tend to "blow up" this region to provide necessary increased surface area for fluid removal as shown in Fig. 12.

Without injection the recirculation zone is relatively small, with stagnation points at A and B. The turning angle to region 1 is large, implying low pressure. Finally, a strong shock is required to redirect the flow to region 2. As shown in the lower figure, the expanded recirculation region contains stagnation points at A, where total pressure of injectant matches that of recirculating flow and B, at the rear of the recirculation zone. The larger recirculation zone requires smaller expansions of the inviscid flow with higher pressures and weaker trailing shock with smaller losses.

Such possibilities are the topic of the following experimental efforts.

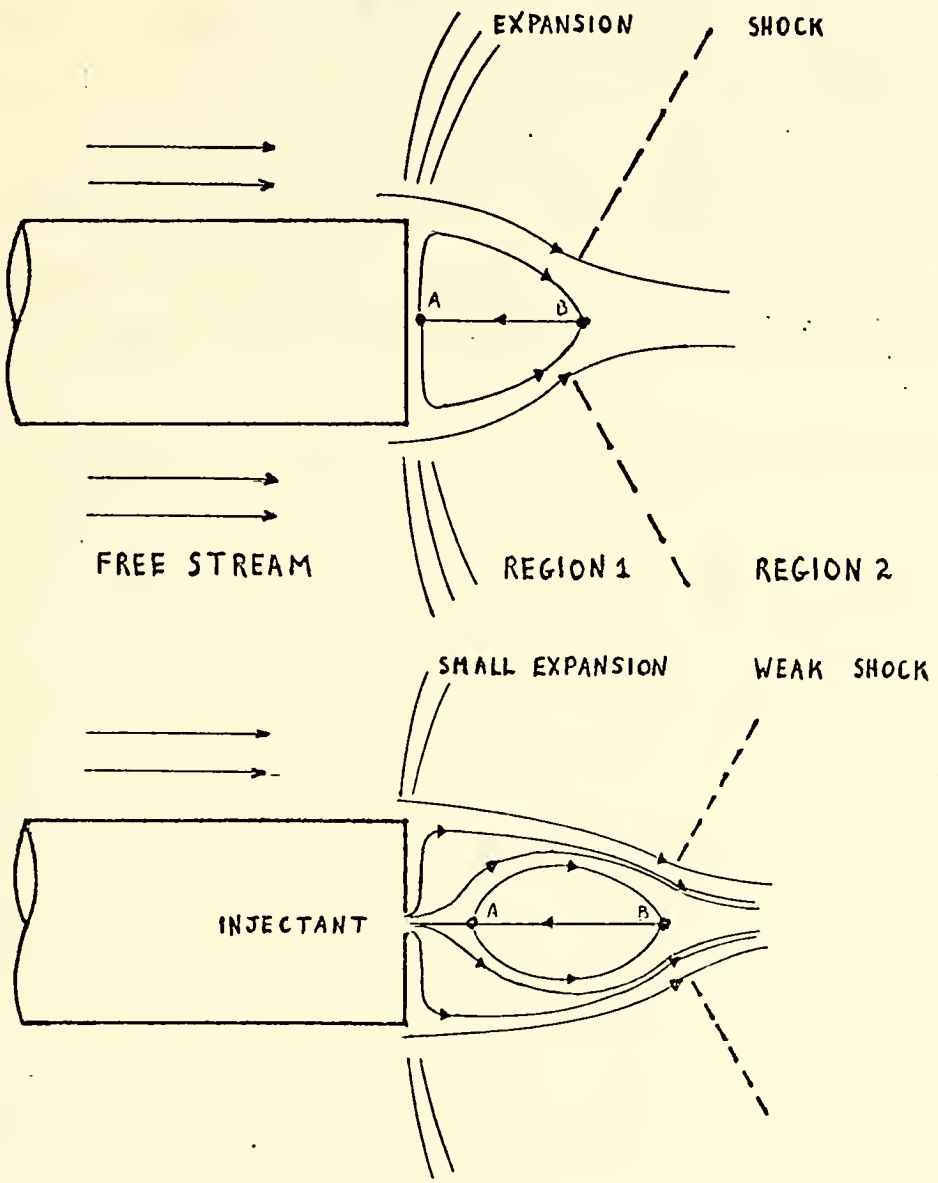

Fig 12

INVISCID EFFECTS

VI. DESCRIPTION OF APPARATUS AND EXPERIMENTS

A. APPARATUS

Complete details on construction and operation of the experimental equipment are contained in References 4 and 5. The basic problem involves simulation of a 5-inch projectile at 23,000 feet with free stream Mach number of 2.0. Reynolds number based on diameter was 1.51×10^6 with turbulent boundary layer thickness to diameter ratio at the base of .0164. The effects of free stream combustion and base injection were studied.

A photograph and schematic of the test facility are illustrated in Figs. 13 and 14.

Three hundred PSIG air is controlled by the globe and pressure reducer valves and ducted through 4-inch pipe around a 90° elbow. Flow straighteners stabilize the flow before reaching the supersonic nozzle. The overhead hood allows venting of the flow. The projectile itself is simulated by the cylinder located concentric with the nozzle. Nitrogen injection is accomplished by means of a portable nitrogen bottle with pressure reducer valve as a source. Injectant is ducted by plastic tubing to plenum chamber within the cylinder and finally exits through the base injection port. Two pressure taps located at the base of the cylinder, one slightly upstream of the base and one within the injectant plenum chamber, record via manometer board the pressures in these areas. Details of the cylinder are shown in Figs. 15 and 16. A schlieren and Polaroid camera provide photographic data.

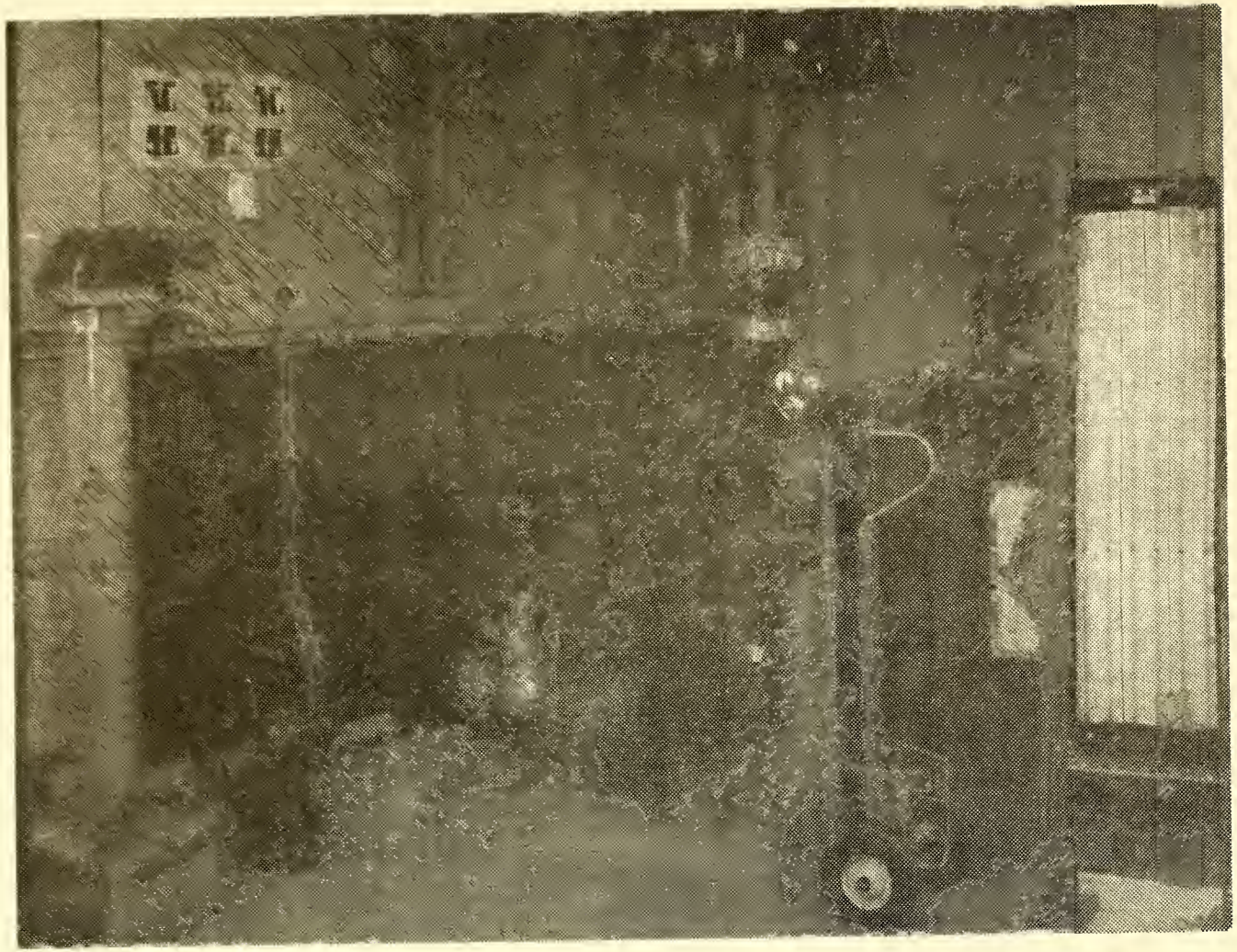

FIG 13

TEST FACILITY

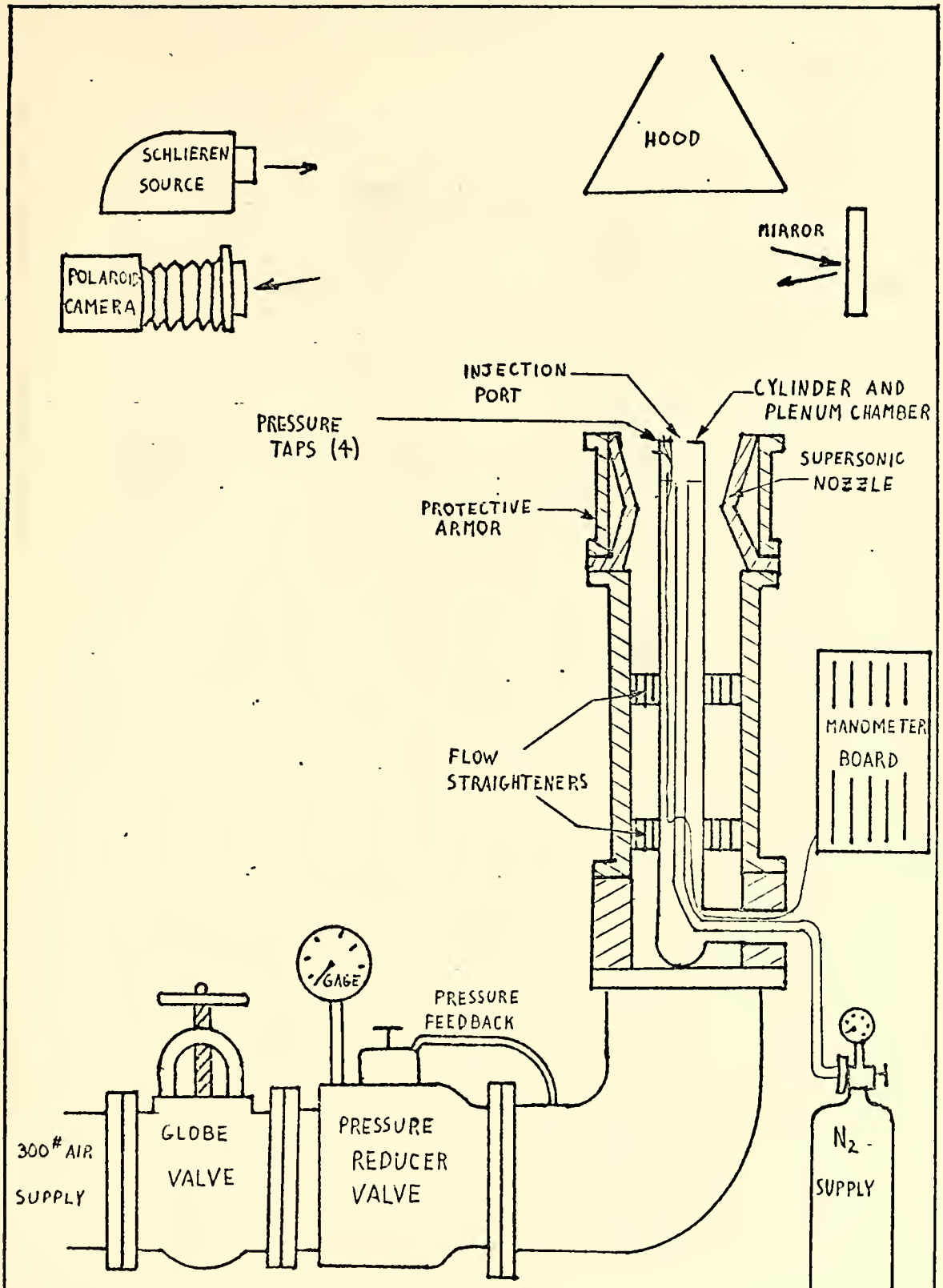

FIG 14

FACILITY SCHEMATIC

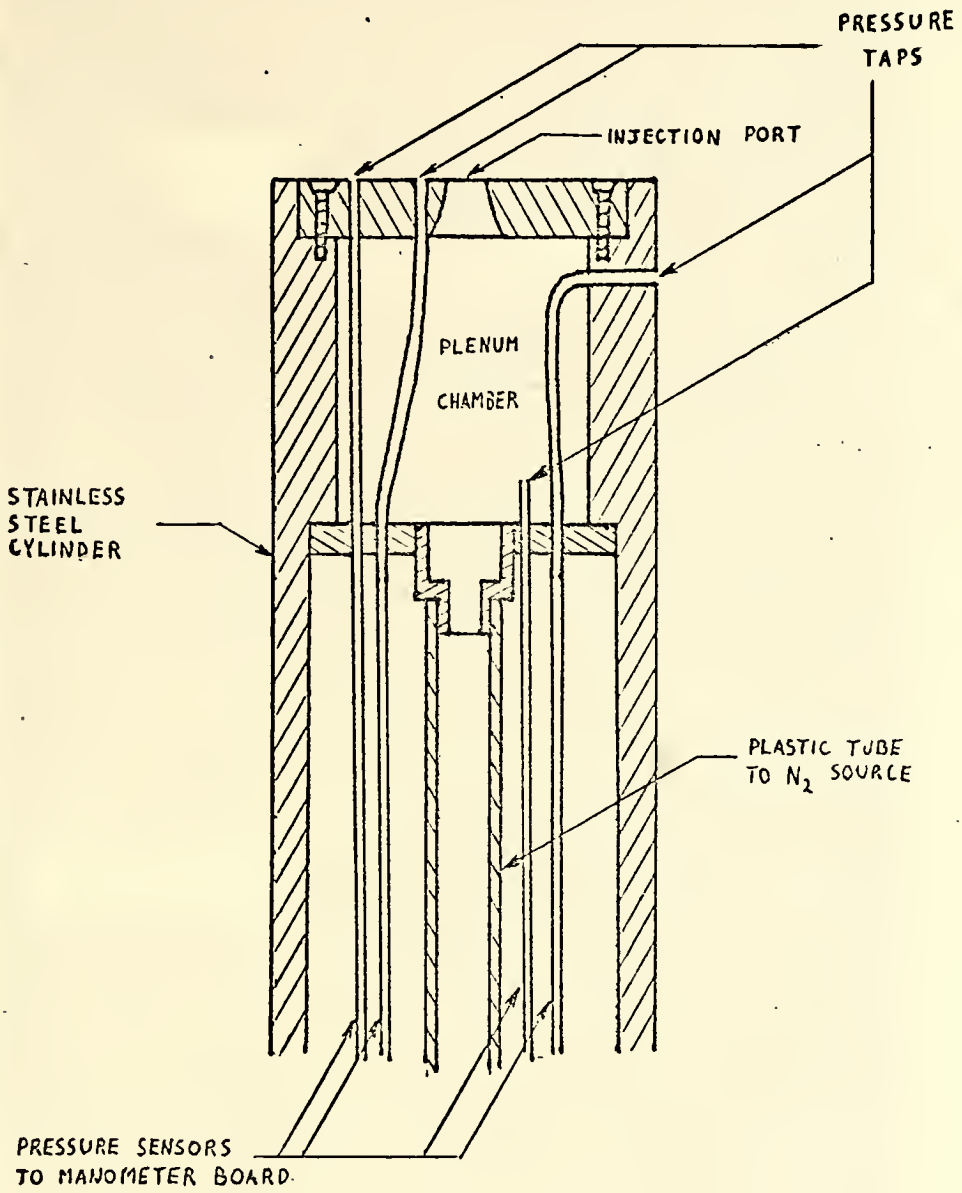

Fig 15

CYLINDER SCHEMATIC

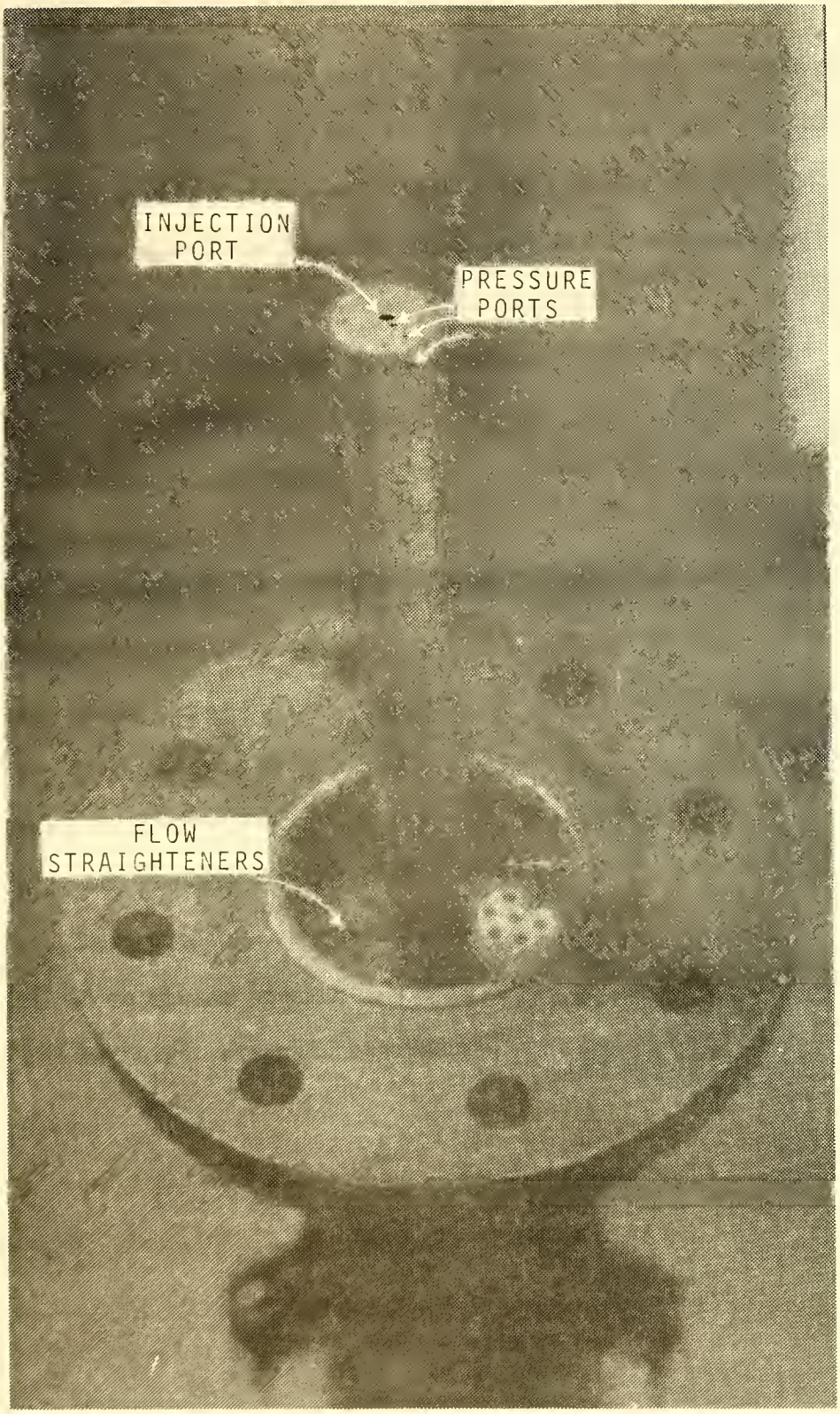

FIG 16

CYLINDER ASSEMBLY

B. EXPERIMENTAL PROCEDURE

Experimental data were derived from a series of tests wherein various combinations of base injection and free stream burning were compared. Compression waves from free stream burning were simulated by varying contours of the supersonic nozzles. Base injection was accomplished by varying the flow of nitrogen through the base injection port.

The experiments, themselves, consisted of:

1. Charge the 300PSIG air supply
2. Note ambient conditions
   a. Temperature
   b. Pressure
3. Set up desired flow rates
   a. Bleed gas
   b. Main air supply
4. Take schlieren photograph
5. Note manometer readings
   a. Base pressure, static, 2 sources, P_B.
   b. Free stream pressure, static, P_∞
   c. Injectant stagnation pressure, $P_{T_{inj}}$
6. Secure systems

VII. EXPERIMENTAL RESULTS

As had been stated earlier, the experiment sought to simulate a 5-inch projectile at 23,000 feet.

Modeling parameters included:

1. Geometric similarity: injection port diameter to base diameter ratio of 0.078.
2. Free stream Mach number = 2.0
3. Injectant stagnation pressure to base pressure ratio equates injectant Mach numbers for model and projectile
4. Free stream Reynolds number = 1.5×10^6
5. Match injectant Reynolds numbers based on injection port diameter by assuming appropriate total temperatures for projectile injectant.
6. Momentum flux of injectant to free stream ratio: $\frac{(\rho U^2 A)_{\text{injectant}}}{(\rho U^2)_{\infty} A_{\text{base}}}$
7. Ratios of fluid specific heats for model and projectile = 1.4
8. Assuming that the above conditions may be suitably matched, flow similarities are presumed, resulting in similar base pressure ratios, $\frac{P_B}{P_\infty}$.

Due to the infinite number of combinations of base injection and free stream combustion, each with its own particular effects, efficiency rather than total thrust was chosen for optimization. For this reason specific impulse, I_{sp}, was selected as the measure of effectiveness.

Reference conditions were established using a nozzle to provide a relatively uniform flow. No combustion or injection was allowed. From these basic data one could determine the effects of the various flow modifiers.

The results of this initial run are shown in Fig. 17. The base pressure ratio, P_B/P_∞, in this case was found to be 0.659. This corresponds to a total base drag of 39.8 pounds at altitude. Thrust was defined as the difference in base drag as the flow is modified. I_{sp} is then determined from the flow rates of injectant or fuel required to attain this drag reduction.

The drag reduction is due to two components: increase in base pressure, and injectant momentum flux. The latter is approximately equal to $(P_{T_{inj}} - P_B) \cdot A_{inj}$ where A_{inj} is the cross sectional area of the injection port.

Figures 18-22 contain additional schlieren photographs of results derived from varying base injection rates without effects of free stream combustion.

Table III summarizes numerical data derived from these runs.

In order to match Reynolds numbers it was necessary to assume $T_{T_{inj}}$ of about 720°R for the actual projectile while model $T_{T_{inj}}$ was about 530°R.

From data presented in Figs. 23-26, it becomes readily apparent that total thrust as well as I_{sp} reaches a maximum value in the mid ranges of the test regions. Due to the small component of reactive thrust, it appears that momentum flux plays a small part until it reaches a sufficiently large value where, instead of aiding the situation, flow distortions cause a net increase in base drag. A proposed cause for this is indicated in Fig. 27. Information for this figure was derived from general recirculation theory, with the aid of water table analysis.

With no base injection, (Part A) the base flow pattern follows commonly accepted theory. There is no thrust (thrust is used to denote increased P_B) in this case, as shown in Fig. 25. Small rates of base

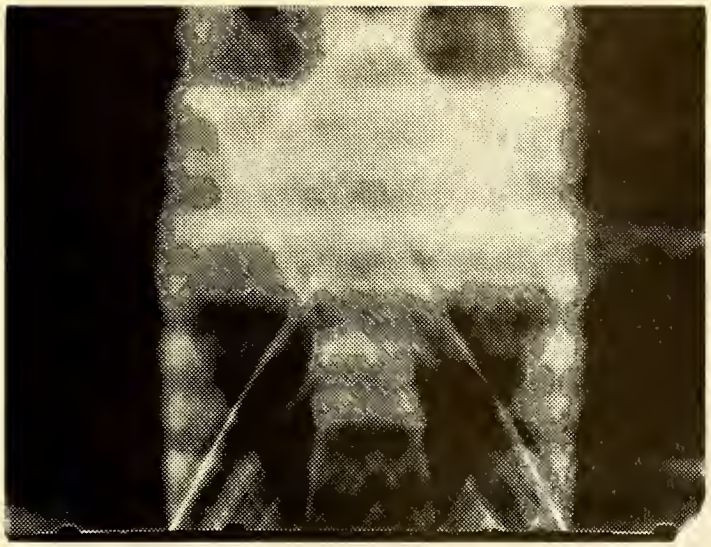

FIG 17

PHOTOGRAPH OF FIRST RUN WITH NO INJECTION OR COMPRESSION

FIG 18

PHOTOGRAPH WITH $\frac{P_B}{P_{T_{inj}}}$ .5681

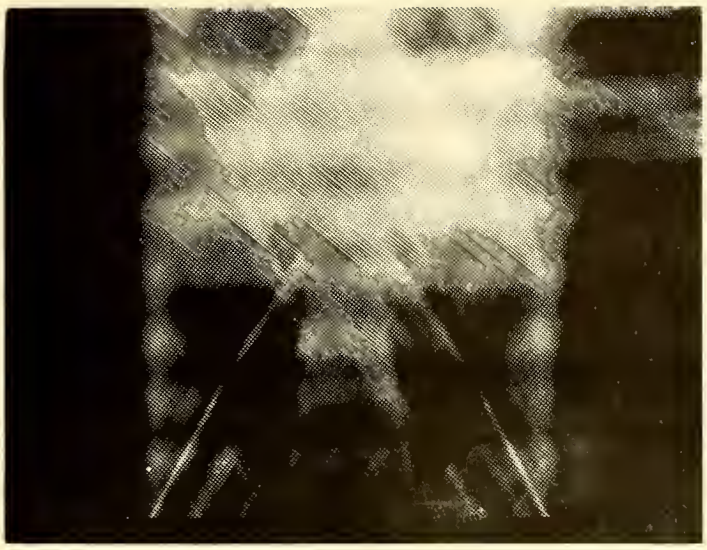

FIG 19

PHOTOGRAPH WITH

$\frac{P_B}{P_{T_{inj}}} = .5677$

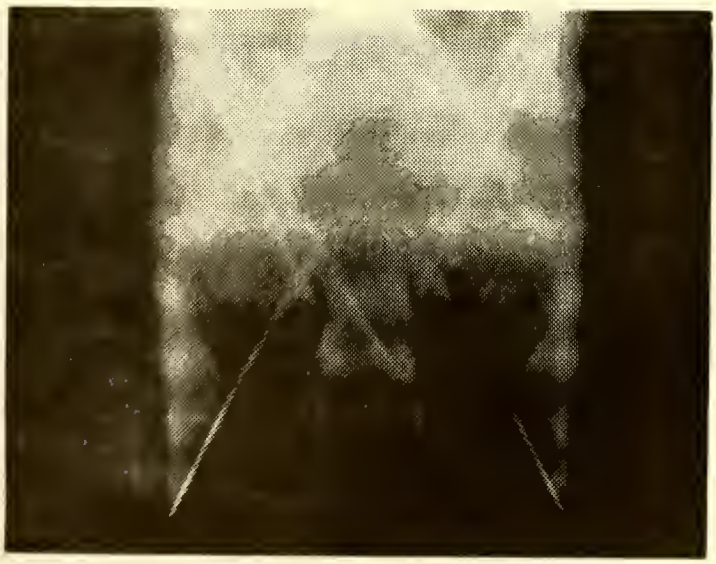

FIG 20

PHOTOGRAPH WITH

$\frac{P_B}{P_{T_{inj}}} = .4513$

FIG 21

PHOTOGRAPH WITH

$\frac{P_B}{P_{T_{inj}}} = .4135$

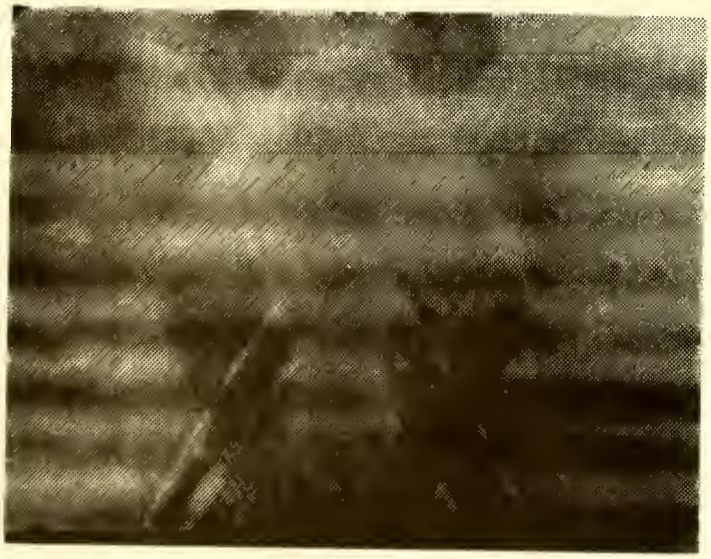

FIG 22

PHOTOGRAPH WITH

$\frac{P_B}{P_{T_{inj}}} = .3297$

TABLE III. EXPERIMENTAL DATA, BASE INJECTION ALONE

$\frac{P_B}{P_{T_{inj}}}$	Figure	M_{inj}	Re_{inj} Model	Re_{inj} Projectile	$\frac{(\rho U^2 A)_{inj}}{(\rho U^2)_\infty A_{base}}$	$\frac{P_B}{P_\infty}$
.6114	none	.87	41542	43392	.00076	.705
.5681	18	.94	44375	45824	.00087	.701
.5677	19	.94	44678	45824	.00087	.709
.4513	20	1.0	57582	58893	.00119	.725
.4135	21	1.0	61809	63402	.00128	.742
.3297	22	1.0	77521	79745	.00160	.742
.3155	none	1.0	84459	86227	.00174	.719
.3105	none	1.0	83821	85663	.00173	.709
.3076	none	1.0	83821	85663	.00173	.710

$\frac{P_B}{P_{T_{inj}}}$	Reaction Thrust	Pressure Thrust	Total Thrust	$\dot{m}_{inj}$	I_{sp} Total	$\frac{(\rho UA)_{inj}}{(\rho U)_\infty A_{base}}$
.6114	.32	5.36	5.68	.0153	371	.00149
.5681	.38	4.89	5.27	.0162	325	.00158
.5677	.38	5.82	6.20	.0162	382	.00158
.4513	.63	7.69	8.32	.0208	400	.00203
.4135	.75	9.68	10.43	.0224	465	.00218
.3297	1.07	9.68	10.75	.0282	381	.00275
.3155	1.11	6.99	8.10	.0305	265	.00297
.3105	1.12	5.82	6.94	.0303	229	.00295
.3076	1.13	5.94	7.07	.0303	233	.00295

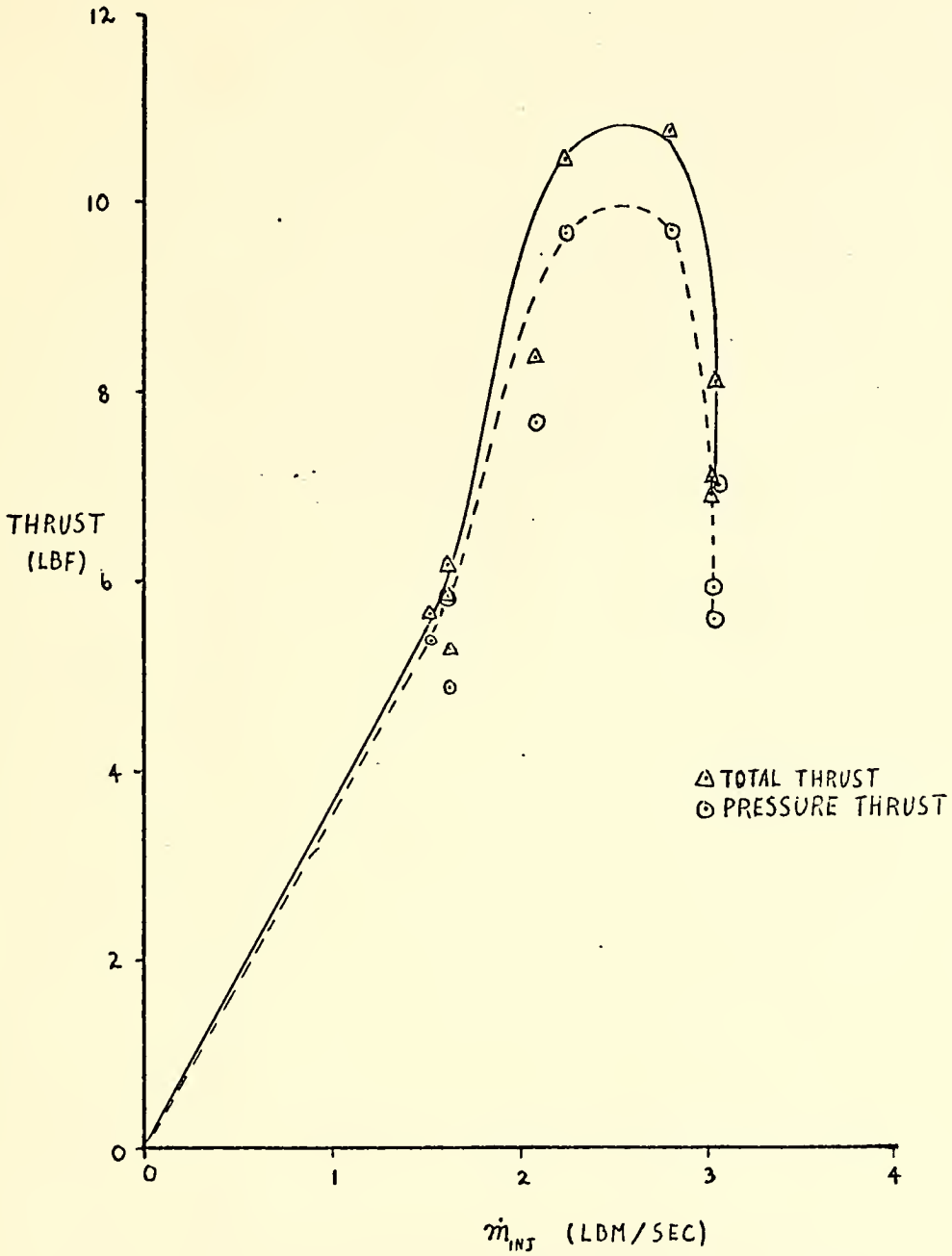

Fig 23

PLOT OF THRUST vs INJECTANT FLOW

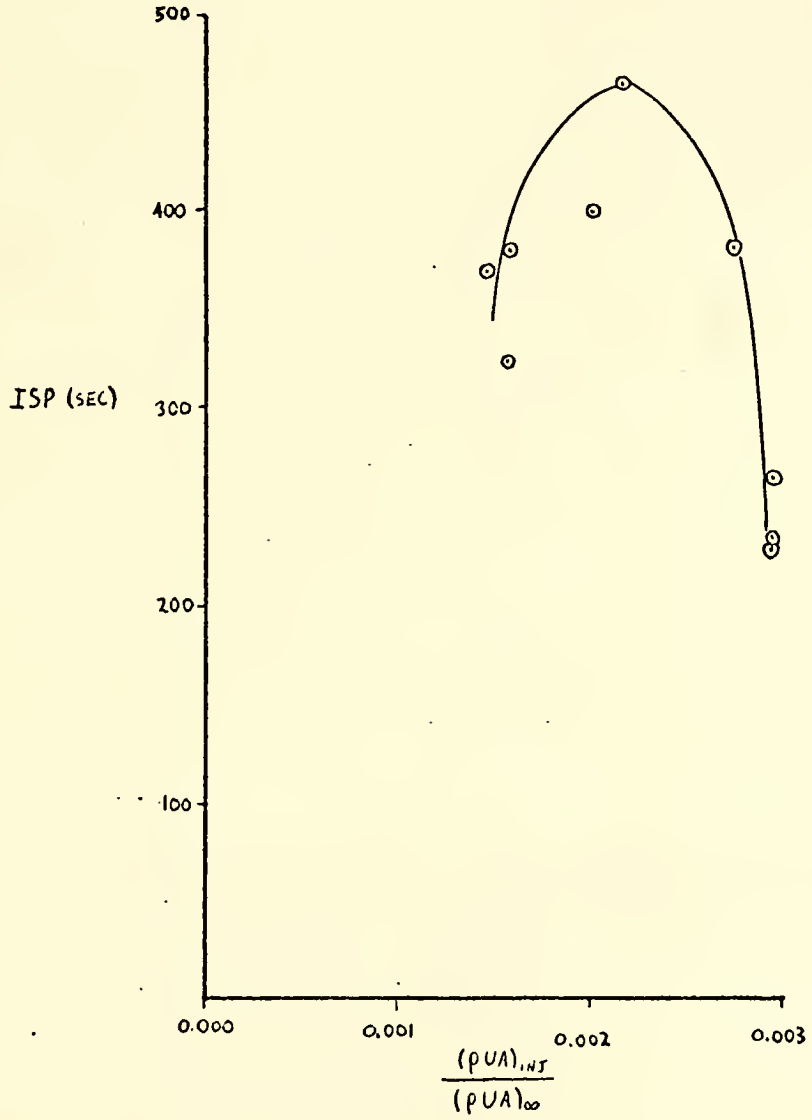

Fig 24

PLOT OF I_{sp} vs NORMALIZED INJECTANT FLUX

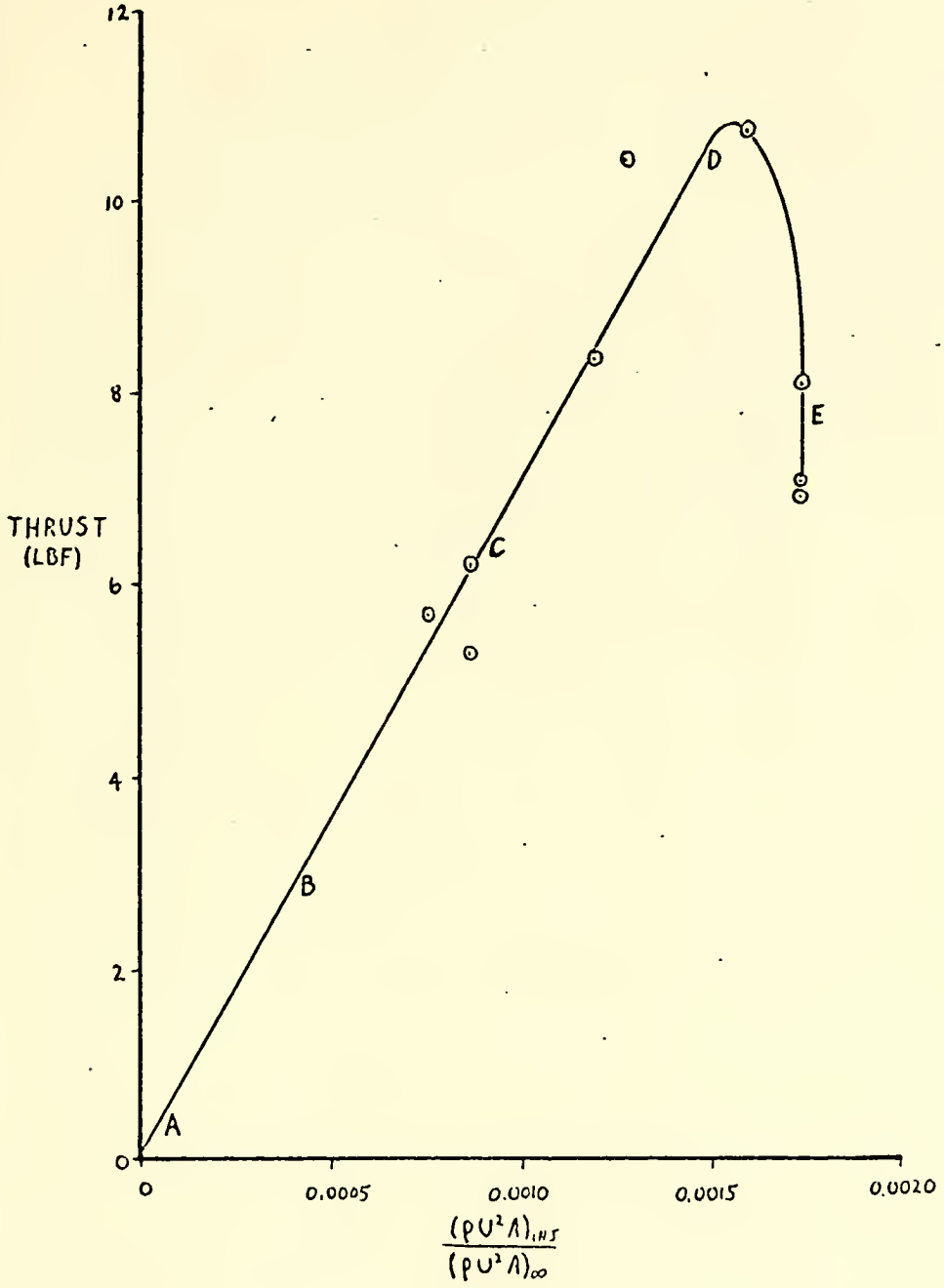

Fig 25

PLOT OF THRUST vs NORMALIZED MOMENTUM

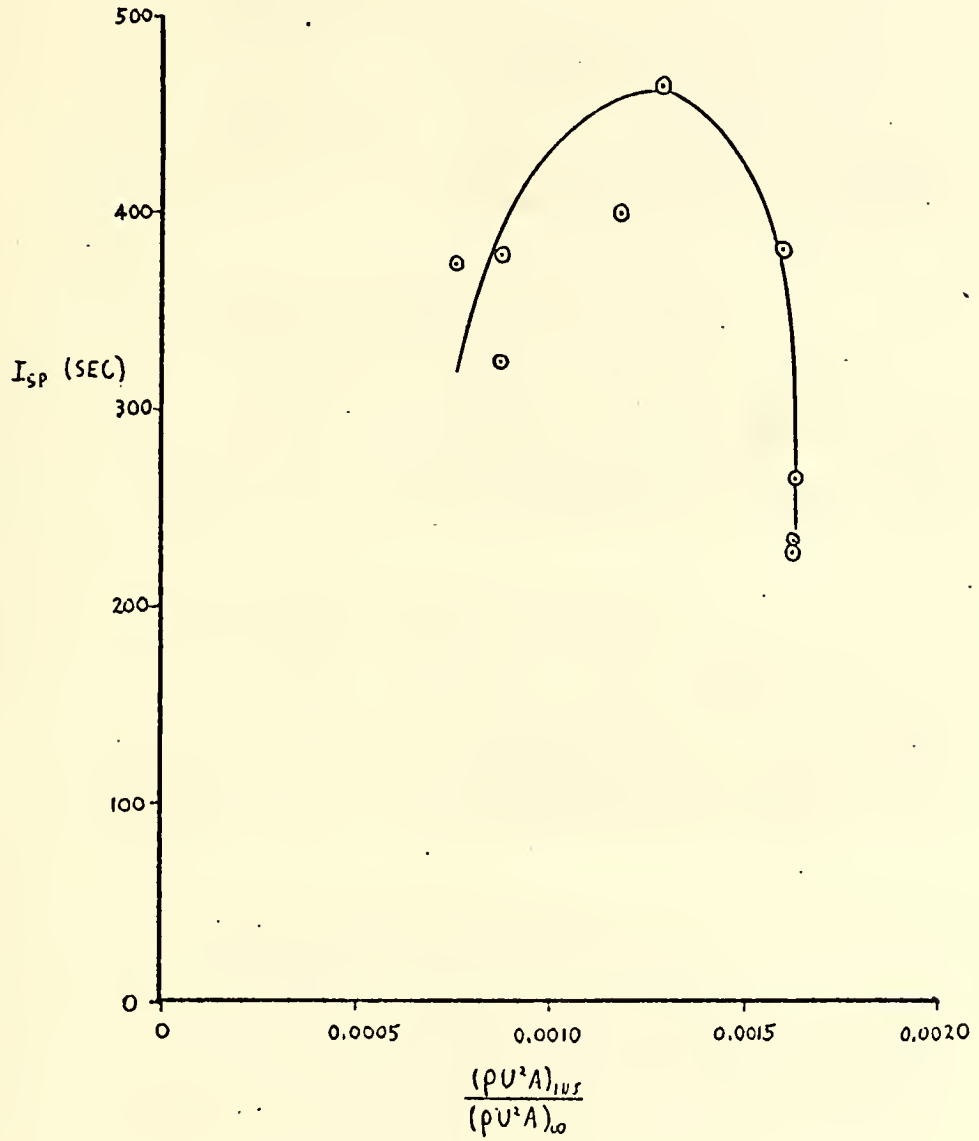

Fig 26

PLOT OF Isp vs HORMALIZED MOMENTUM

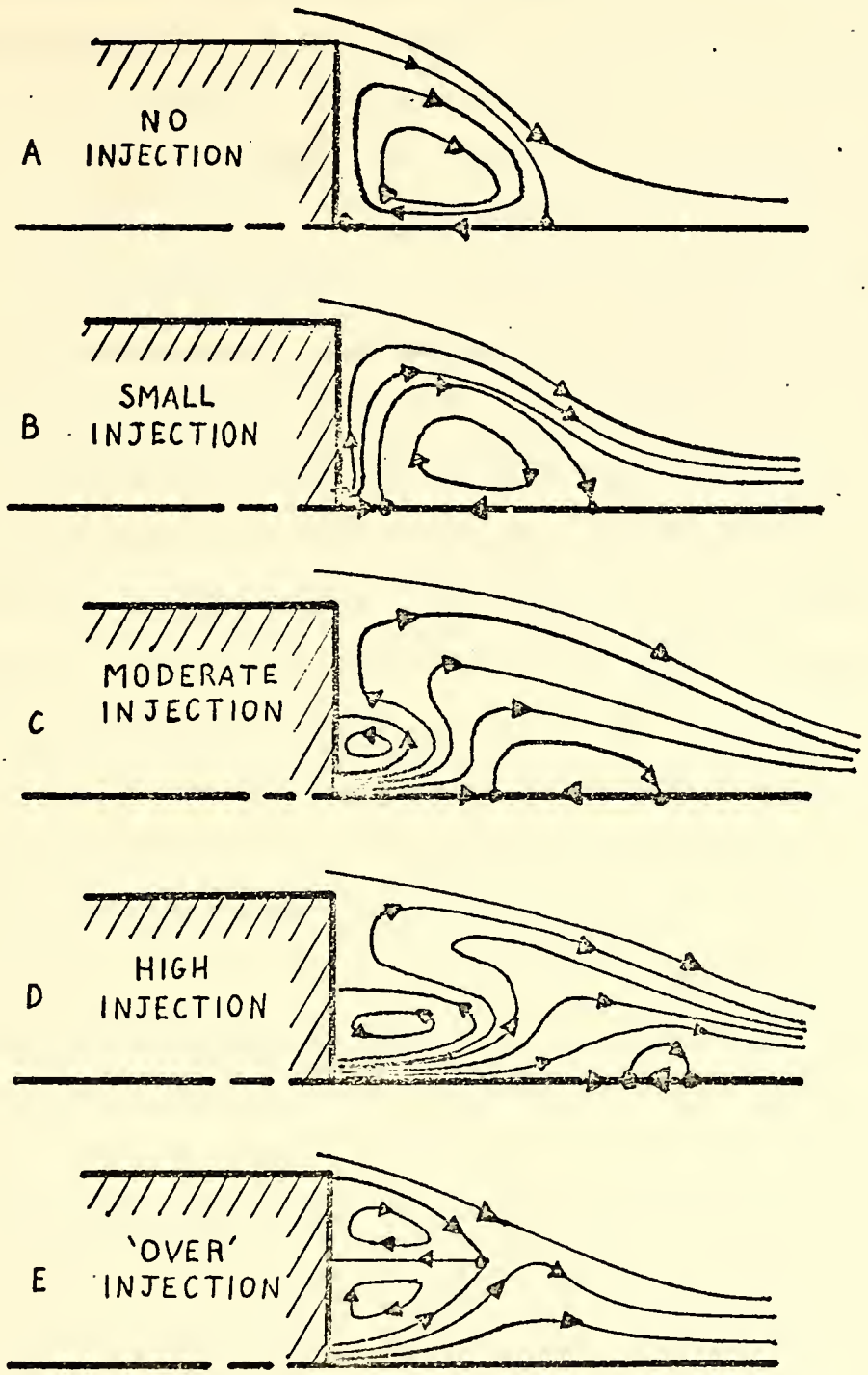

Fig 27

MOMENTUM RESULTS

injection (Part B) begin to require shear layer scavenging action. The flow deflection angles decrease and base pressure increases. Futhermore, the forward stagnation point in the recirculation region is being driven aft. Increased injection (Part C) causes a small recirculation zone to form within the injectant fluid. The forward stagnation point continues to move aft and thrust increases. As injection rates increase further (Part D), the basic recirculation zone continues to shrink in size as thrust approaches a maximum. Finally, injection rates reach a point (Part E) where the original recirculation region stagnation pressures are overcome and mass exits directly through the wake area. Free shear scavenging decreases and flow deflection angles increase, resulting in marked decreases of base pressure. The optimum rate of base injection would appear to balance stagnation pressures with injectant momentum flux, requiring the strongest scavenging action.

Having compiled the data demonstrating the effects of base injection alone, the combined effects of base injection in conjunction with free stream combustion were sought. Reference 11 contains a summary of experimental results using substantially the same test equipment wherein free stream combustion was simulated. The configuration yielding the highest I_{sp} was selected for the combined studies. This consisted of a combustion length to cylinder radius ratio of 0.72 located so that the first full compression wave inpinged on the base flow area one half radius downstream of the body. This resulted in a base pressure ratio, P_B/P_∞, of 0.993 and $I_{sp} = 525$. A similar series of experiments was run varying the mass injection in the base. Table IV lists the results of these experiments. A fuel flow rate for free stream combustion of .072 lbm/sec was assumed. This corresponds with the properties of ARC - 163, heat release of 7200 BTU/lbm, and $\Delta T = 3060^{\circ}F$ at stoichiometric burning.

The results obtained using the fixed pattern of free stream combustion and varying the base injection rates are listed in Table IV. Figures 28-36 contain schlieren-derived photographs of selected runs. It should be noted here that, unlike the first series of photographs, the near wake areas are obscured by the nozzle assembly and one can see only the compression wave reflection from the base flow area.

From Figs. 37 and 38, it is apparent that small amounts of mass injection into the base flow area under external compression do not decrease drag as effectively as without external compression. Increased mass injection results in a nearly level thrust curve and decreasing I_{sp}. The effects of mass injection and external compression are not additive. External compression, when present, dominates the base flow problem.

TABLE IV. EXPERIMENTAL DATA,

BASE INJECTION COMBINED WITH FREE STREAM COMBUSTION

$\frac{P_B}{P_{T_{inj}}}$	Figure	M_{inj}	Re_{inj} Model	Re_{inj} Projectile	$\frac{(\rho U^2 A)_{inj}}{(\rho U^2)_\infty A_{base}}$	$\frac{P_B}{P_\infty}$
no injection	28	0	0	0	0	.991
.808	29	.56	29181	32369	.00042	.979
.719	30	.70	40477	43570	.00068	1.016
.602	31	.88	53090	56485	.00108	.996
.576	32	.92	57603	60689	.00118	1.003
.536	33	.99	66066	66808	.00135	1.005
.483	34	1.00	72919	73617	.00150	1.000
.415	35	1.00	84830	85859	.00175	1.000
.361	36	1.00	97243	98630	.00201	.997

$\frac{P_B}{P_{T_{inj}}}$	Reaction Thrust	Pressure Thrust	Total Thrust	$\dot{m}_{inj}$	$\dot{m}_{fuel}$ (Total)	I_{sp}
no injection	0	37.81	37.81	0	.072	525
.808	.17	37.38	37.55	.01136	.083	452
.719	.28	41.65	41.93	.01612	.088	476
.602	.47	39.42	39.89	.02089	.093	429
.576	.52	40.23	40.75	.02195	.094	434
.536	.62	40.43	41.05	.02361	.096	428
.483	.76	39.82	40.58	.02602	.098	414
.415	1.00	39.82	40.82	.03035	.102	400
.361	1.25	39.41	40.66	.03486	.107	380

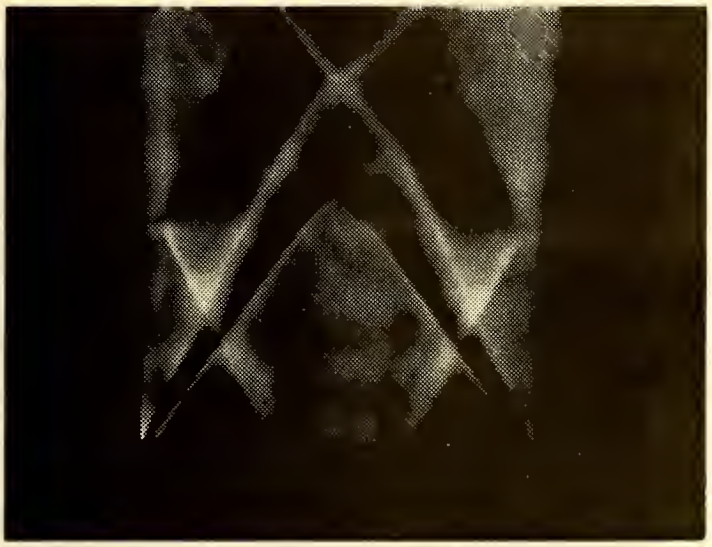

FIG 28

PHOTOGRAPH WITH $\dot{m}_{inj}$ 0

EXTERNAL COMPRESSION

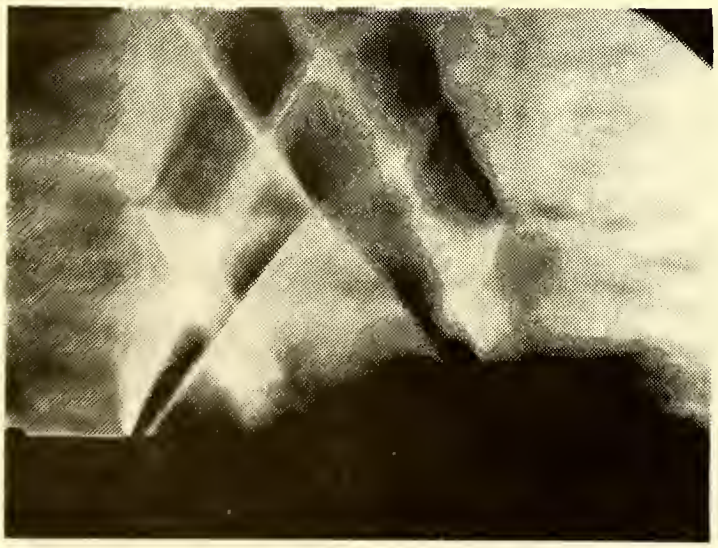

FIG 29

PHOTOGRAPH WITH

$\frac{P_B}{P_{T_{inj}}} = .808$

EXTERNAL COMPRESSION

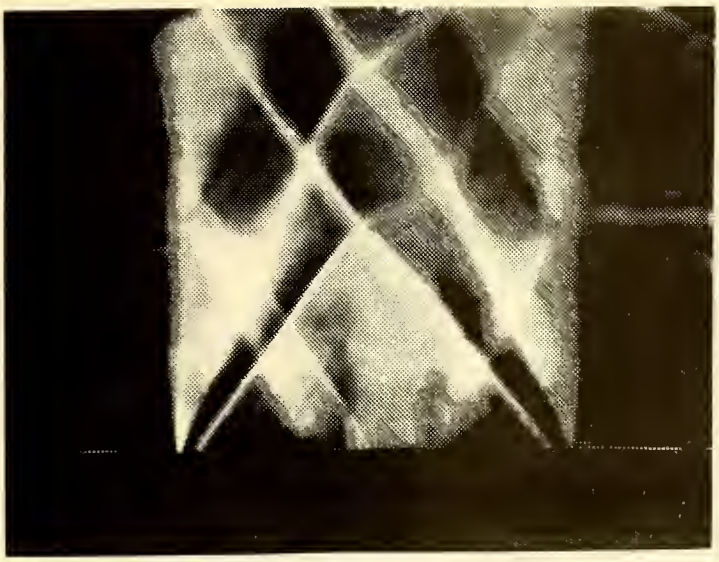

FIG 30

PHOTOGRAPH WITH

$\frac{P_B}{P_{T_{inj}}} = .719$

EXTERNAL COMPRESSION

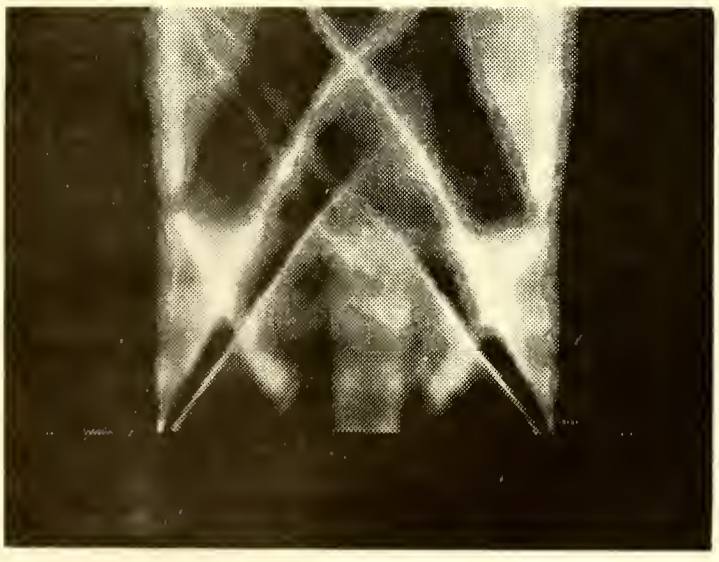

FIG 31

PHOTOGRAPH WITH

$\frac{P_B}{P_{T_{inj}}} = .602$

EXTERNAL COMPRESSION

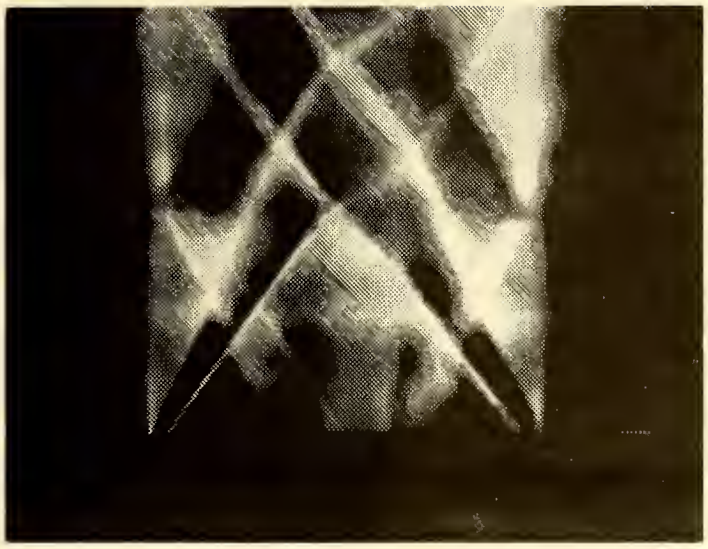

FIG 32

PHOTOGRAPH WITH

$\frac{P_B}{P_{T_{inj}}}$ .576

EXTERNAL COMPRESSION

FIG 33

PHOTOGRAPH WITH

$\frac{P_B}{P_{T_{inj}}}$ = .536

EXTERNAL COMPRESSION

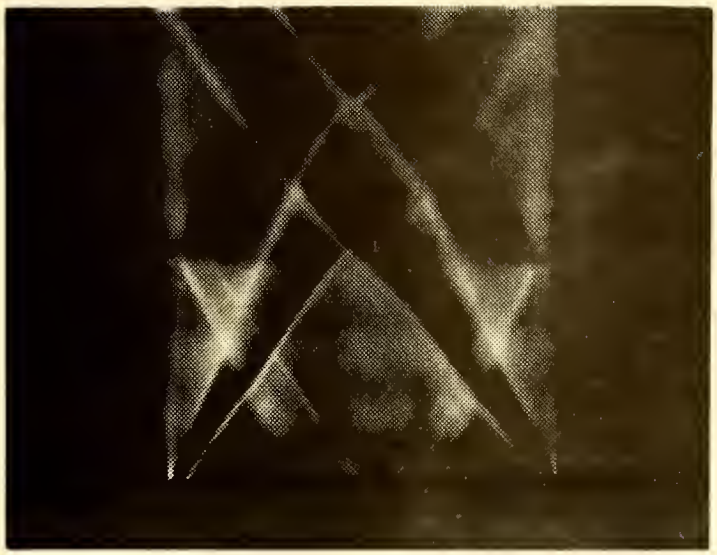

FIG 34

PHOTOGRAPH WITH

$\frac{P_B}{P_{T_{inj}}}$ .483

EXTERNAL COMPRESSION

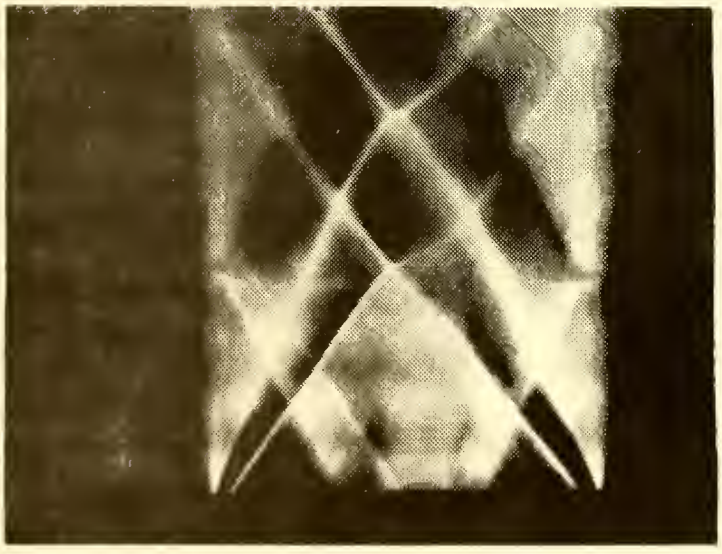

FIG 35

PHOTOGRAPH WITH

$\frac{P_B}{P_{T_{inj}}}$ - .415

EXTERNAL COMPRESSION

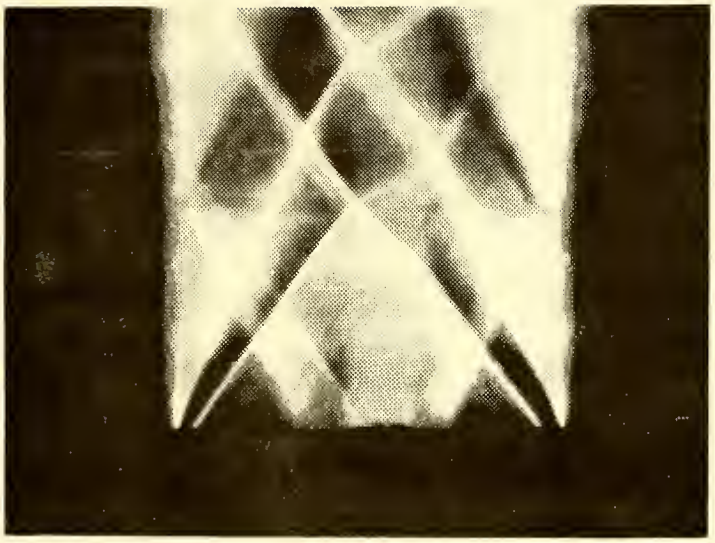

FIG 36

PHOTOGRAPH WITH $\frac{P_B}{P_{T_{inj}}}$ = .361, EXTERNAL COMPRESSION

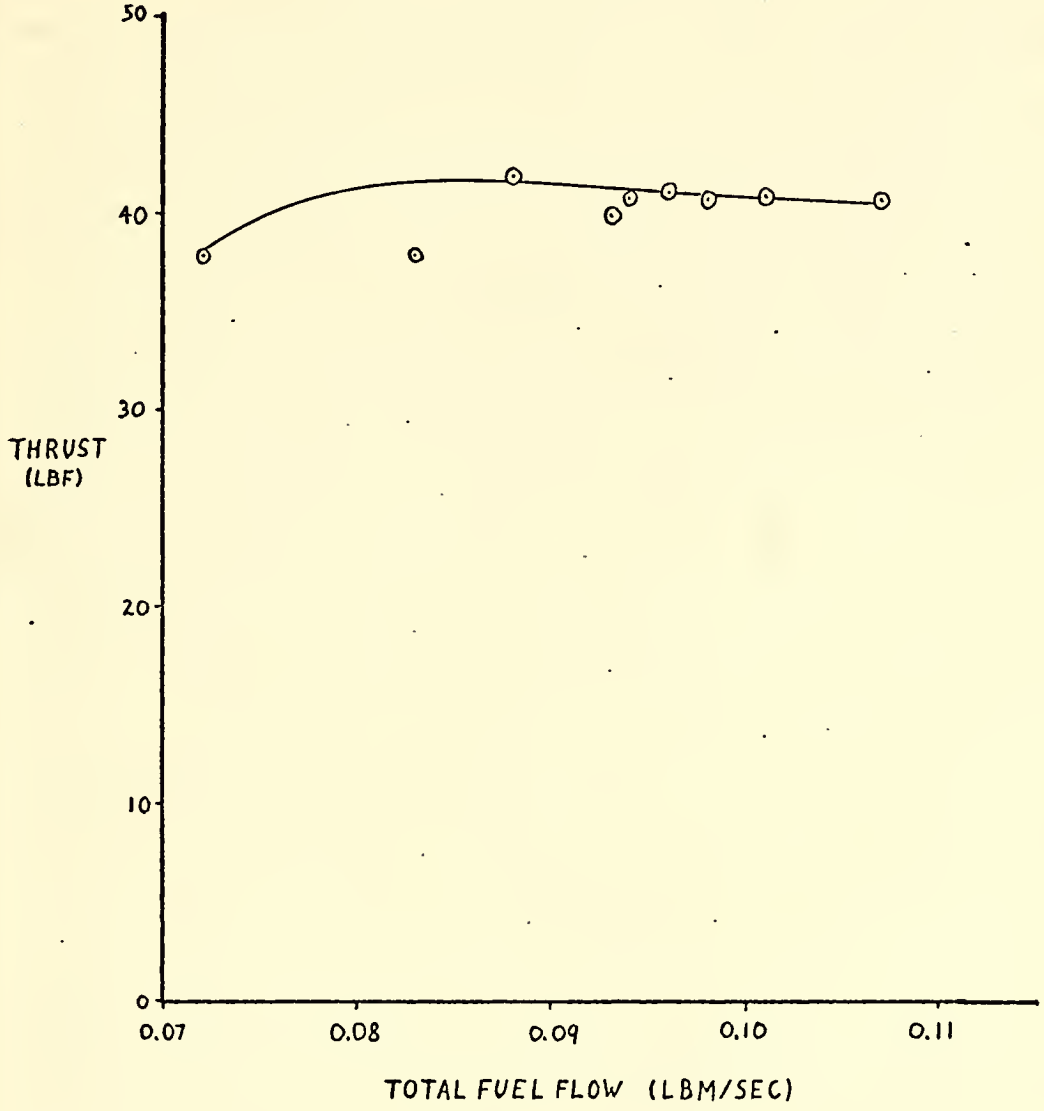

FIG 37

PLOT OF THRUST vs FUEL FLOW

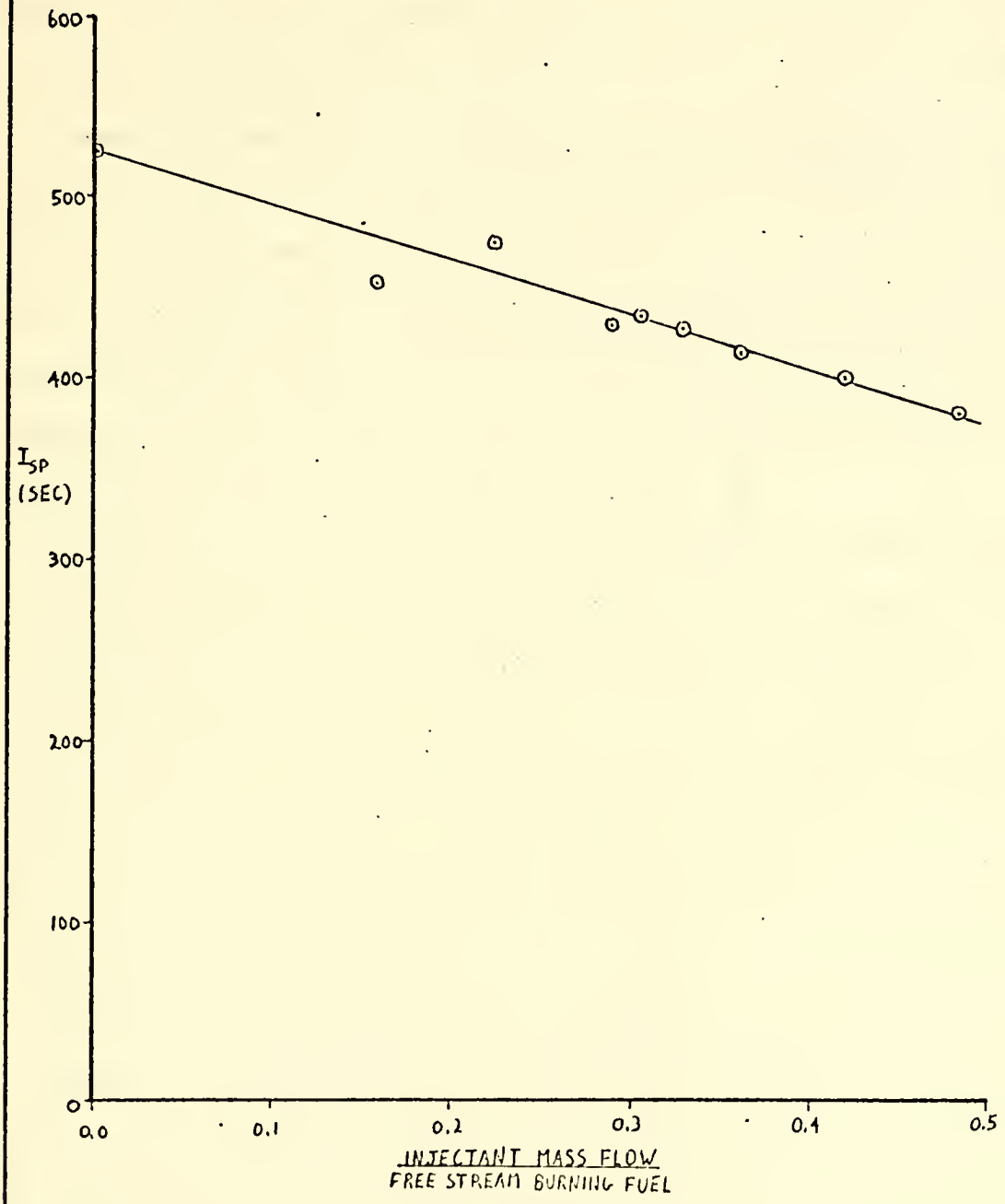

FIG 38

PLOT OF Isp vs FLOW RATIO

VIII. CONCLUSIONS AND RECOMMENDATIONS

Results of analytic studies of the base flow problem, as shown in Tables I, II and summarized in Fig. 9, indicate that the trailing shock dominates base drag. Experimental studies sought to reduce this drag by decreasing the strength of the shock.

A base pressure ratio of 0.659 was achieved experimentally without injection. Table III, a summary of experimental data, indicates a maximum base pressure ratio of 0.742 was achieved by injection of cold nitrogen, at an effective I_{sp} of 465 seconds. Figures 23 and 25, however, show that achieved thrust reaches a peak and falls off rapidly with increased mass injection rates. A proposed solution, derived in part from water table analysis, is indicated in Fig. 27.

References 7 and 8 studied the effects of compression waves, generated by external burning, on base drag. Base injection was combined with external compression. Results, as shown in Table IV, Figs. 37 and 38, are in general agreement with prior studies and indicate that base injection does not greatly affect base drag when external compression is present. Under the test condition, I_{sp} tends to decrease linearly with base injection, demonstrating that external compression and base injection effects are not linearly additive.

Drag reductions obtained by mass injection, although limited, may be accomplished with no new technology, as shown by the use of tracer rounds. The associated economy of design and materials appears to provide at least an attractive interim solution for the base drag problem.

LIST OF REFERENCES

1. Greenwood, G. H., Measurements of Drag, Base Pressure and Base Aerodynamic Heat Transfer Appropriate to 8.5° Semi-Angle Sharp Cones in Free Flight at Mach Numbers from 0.8 to 3.8, Ministry of Technology Aeronautical Research Council Current Paper No. 958, 1967.

2. Sedney, R., Review of Base Drag, BRL Report 1337, October 1966.

3. Chapman, D. R., An Analysis of Base Pressures at Supersonic Velocities and Comparison with Experiment, NACA TN 2137, July 1950.

4. Schlichting, H., Boundary Layer Theory, p. 125-134, McGraw-Hill, 1968.

5. Strahle, W. C., Theoretical Consideration of Combustion Effects on Base Pressure in Supersonic Flight, Twelfth Symposium on Combustion Institute, Pittsburgh, Pa., pp. 1163-1173, 1969.

6. Fuhs, A. E., Quasi Area Rule for Heat Addition in Transonic and Supersonic Flight Regimes, AFAPL: TR-72-10, August 1972.

7. Caswell, G. J., Base Drag Reduction by External Burning, Master's Thesis, Naval Postgraduate School, Monterey, Calif., September 1973.

8. Naber, M. E., Investigation of the External Burning Assisted Projectile, Master's Thesis, Naval Postgraduate School, Monterey, Calif., September 1973.

9. Collins, D. J., Lees, L. and Roshko, A., Near Wake of a Hypersonic Blunt Body with Mass Addition, AIAA Journal Vol. 8, No. 5, May 1970.

10. Lewis, J. E. and Chapkis, R. L., Mean Properties of the Turbulent Near Wake of a Slender Body with and without Base Injection, AIAA Journal, Vol. 7, No. 5, May 1969.

11. Fuhs, A. E., Smithey, W., Naber, M., Caswell, G., External Burning Assisted Projectile Theory and Experiment, AIAA Paper, No. 73-1193, November, 1973.

INITIAL DISTRIBUTION LIST

		No. of Copies
1.	Defense Documentation Center Cameron Station Alexandria, Virginia 22314	2
2.	Library, Code 0212 Naval Postgraduate School Monterey, California 93940	2
3.	Professor A. E. Fuhs Department of Aeronautics Naval Postgraduate School Monterey, California 93940	5
4.	LTjg Gary J. Caswell, USN 399 Troy Aurora, Colorado 80010	3
5.	Dr. Warren Strahle Aerospace Engineering Georgia Institute of Technology Atlanta, Georgia 30332	1
6.	Mr. Dominic J. Monetta Gun Systems Engineering Naval Ordnance Station Indian Head, Maryland 20640	2
7.	Dr. Alan Roberts Gun Systems Engineering Naval Ordnance Station Indian Head, Maryland 20640	2
8.	Dr. Frederick Billig Applied Physics Laboratory Johns Hopkins University 8621 Georgia Avenue Silver Springs, Maryland 20910	1
9.	CDR William Smithey SMC, Box 2348 Naval Postgraduate School Monterey, California 93940	3
10.	Dr. James S. Holdhusen Vice President FluiDyne Engineering Corporation 5900 Olsen Highway Minneapolis, Minnesota 55422	1

11. Mr. Thomas Curran — 1
Chief of Ramjet Technology Branch
Air Force Applied Physics Laboratory
Wright Patterson Air Force Base, Ohio 45433

12. LT Noel P. Horn, USN — 3
SMC, Box 1183
Naval Postgraduate School
Monterey, California 93940

13. Dr. Richard Weiss
Air Force Rocket Propulsion Laboratory
Edwards Air Force Base, California

14. Professor John Clarke — 1
Cranfield Institute of Technology
Bedford, England

15. Dr. E. G. Broadbent
Royal Aeronautical Establishment
Farnborough, England

16. Chairman, Department of Aeronautics — 1
Naval Postgraduate School
Monterey, California 93940

17. Dr. Ing. G. Winterfeld — 1
D F V L R
Institut f. Luftstrahlantriebe
505 Porz-Wahn, Linder Höhe, Germany

18. LT Naber — 1
RT. 1, Box 1048
Sequim, Washington 98382

SECURITY CLASSIFICATION OF THIS PAGE (When Date Entered)

REPORT DOCUMENTATION PAGE

READ INSTRUCTIONS BEFORE COMPLETING FORM

1. REPORT NUMBER

2. GOVT ACCESSION NO.

3. RECIPIENT'S CATALOG NUMBER

4. TITLE (and Subtitle)

Investigation of Supersonic Projectile Drag Reduction Using Base Injection and Free Stream Combustion

5. TYPE OF REPORT & PERIOD COVERED

Master's Thesis; March 1974

6. PERFORMING ORG. REPORT NUMBER

7. AUTHOR(s)

Noel Paul Horn

8. CONTRACT OR GRANT NUMBER(s)

9. PERFORMING ORGANIZATION NAME AND ADDRESS

Naval Postgraduate School
Monterey, California 93940

10. PROGRAM ELEMENT, PROJECT, TASK AREA & WORK UNIT NUMBERS

11. CONTROLLING OFFICE NAME AND ADDRESS

Naval Postgraduate School
Monterey, California 93940

12. REPORT DATE

March 1974

13. NUMBER OF PAGES

65

14. MONITORING AGENCY NAME & ADDRESS(if different from Controlling Office)

Naval Postgraduate School
Monterey, California 93940

15. SECURITY CLASS. (of this report)

Unclassified

15a. DECLASSIFICATION/DOWNGRADING SCHEDULE

16. DISTRIBUTION STATEMENT (of this Report)

Approved for public release; distribution unlimited.

17. DISTRIBUTION STATEMENT (of the abstract entered in Block 20, if different from Report)

18. SUPPLEMENTARY NOTES

19. KEY WORDS (Continue on reverse side if necessary and identify by block number)

Base Drag Reduction
Axisymmetric Heat Addition
Base Injection
Base Flow Entropy Generation
Base Drag
Base Flow

20. ABSTRACT (Continue on reverse side if necessary and identify by block number)

Base drag accounts for nearly half the total drag of a supersonic projectile. A review is presented of early base flow studies. By relating rate of entropy generation to projectile drag, it is demonstrated that the trailing shock dominates base drag. Base injection was selected as the means of weaking this shock. Base pressure, as a function of injectant flow rate, was obtained by means of a free jet wind tunnel with a coaxial, Mach 2.0 nozzle. Base pressure ratio (P_B/P_∞) increases of 13 percent at an effective I_{sp} of

DD FORM 1 JAN 73 1473 EDITION OF 1 NOV 65 IS OBSOLETE
S/N 0102-014-6601

20. (cont'd)

465 seconds were achieved with cold nitrogen. Free stream combustion was simulated by nozzle contour. Base pressure increases due to free stream combustion and base injection were shown not to be additive effects.

Thesis
H795 Horn
c.1 Investigation of supersonic projectile drag reduction using base injection and free stream combustion.
149390